ORIGINAL PAPER

Development and Investigation of Electrochemical and Dielectric Properties of Eco-Friendly Lithium-Ion Conductor Biopolymer Electrolyte for Energy Storage Application

Dara M. Aziz[1] · **Rebar T. Abdulwahid**[2,3] · **Sangar A. Hassan**[1] · **Shujahadeen B. Aziz**[4,5] · **Pramod K. Singh**[6] ·
Bandar A. Al-Asbahi[7] · **Abdullah A. A. Ahmed**[8] · **H. J. Woo**[12] · **M. F. Z. Kadir**[9,10] · **Wrya O. Karim**[11]

Abstract

This study investigates Li$^+$ ion-conducting biopolymer blend electrolytes-based on chitosan (CS) and potato starch (PS) with glycerol plasticization. The advanced techniques including FTIR, impedance, TNM, LSV, and CV were employed to characterize the compositional and electrochemical properties of the solid films. The FTIR analysis indicates significant influence of glycerol on polymer/salt interactions, evidenced by the shift of FTIR bands to lower wavenumbers, signifying an increase in free ions within the host polymer system. Impedance results indicate that plasticizer addition reduces the bulk resistance to an optimum value of 49 Ω. The calculated DC values demonstrate the suitability of the electrolyte for use in energy storage applications (ESAs) with the highest ionic conductivity of 2.01×10^{-4} S cm^{-1}. The high values of both ϵ' and ϵ'' at lower frequencies are due to interfacial polarization and the accumulation of charges, respectively. The sample with the largest plasticizer content has shown the highest ϵ' of 112.4 at 10^5 Hz. The shifting of tan δ peaks to the higher frequency side with the increase of plasticizer indicates an increase in the mobility of cations. The combination of tan δ plot and Argand plot was used to explore the dominant mechanism in ion conduction. The electrochemical studies were performed to detect the ability of the films to be used for EDLC applications. The TNM (t_{ion}=0.947) and LSV (decomposition voltage = 3.1 V) values favor the films for ESAs. The pattern of CV curves at various scan rates established the successful design of the EDLC device. The calculated capacitance from the area under CV curves is sufficiently high. The capacitance was influenced by scan rates and changed from 12.92 to 38.68 F/g.

✉ Rebar T. Abdulwahid
rebar.abdulwahid@univsul.edu.iq

✉ Shujahadeen B. Aziz
shujahadeenaziz@gmail.com

1 Department of Chemistry, College of Science, University of Raparin, Ranya 46012, Kurdistan Region, Iraq

2 Medical Laboratory Analysis Department, College of Health Sciences, Cihan University Sulaimaniya, Sulaymaniyah 46001, Kurdistan Region, Iraq

3 Department of Physics, College of Education, University of Sulaimani, Old Campus, Kurdistan Region, Sulaymaniyah 46001, Iraq

4 Hameed Majid Advanced Polymeric Materials Research Lab., Research and Development Center, University of Sulaimani, Qlyasan Street, Kurdistan Regional Government, Sulaymaniyah 46001, Iraq

5 Department of Physics, College of Science, Charmo University, Chamchamal, Sulaymaniyah 46023, Iraq

6 Center for Solar Cells & Renewable Energy, Department of Physics, Sharda University, Greater Noida 201310, India

7 Department of Physics & Astronomy, College of Science, King Saud University, P.O. Box 2455, Riyadh 11451, Saudi Arabia

8 Center for Hybrid Nanostructures (CHyN) and Fachbereich Physik, Universität Hamburg, 20146 Hamburg, Germany

9 Universiti Malaya Centre for Ionic Liquids (UMCiL), Universiti Malaya, 50603 Kuala Lumpur, Malaysia

10 Department of Physics, Faculty of Science, Universiti Malaya, 50603 Kuala Lumpur, Malaysia

11 Department of Chemistry, College of Science, University of Sulaimani, Kurdistan Regional Government, Qlyasan Street, Sulaimani 46001, Iraq

12 Center for Ionics University of Malaya, Department of Physics, Faculty of Science, Universiti Malaya, Kuala Lumpur, Malaysia

Introduction

Recently, there has been a notable focus on solid polymer electrolytes (SPEs) owing to their versatility and the simplicity of creating them as polymer films. In contrast, conventional synthetic polymers typically come from petroleum sources and are often non-degradable, posing environmental concerns. Consequently, a concerted effort has been made to develop biodegradable polymer electrolytes capable of maintaining high ionic conductivity (σ). These sustainable materials have the potential to replace non-degradable polymers in a variety of applications, offering a more eco-friendly alternative while still meeting the critical requirement of efficient ion conduction [1, 2]. Notably, industrial innovators and researchers have been particularly interested in exploring the electrochemical capabilities of polymer electrolytes (PE) in the context of various device applications, with a focus on fuel cells [3], batteries [4], and supercapacitors [5].

Polymer-based electrolytes are solvent-free setups in which the conduit for ionic conduction is formed by incorporating ionic salts into a polymer framework [6, 7]. Unfortunately, the inherent low σ of polymers limits their applicability, prompting the development of various research methodologies to enhance the ionic conduction and electrochemical properties of these polymer-based electrolytes. These approaches encompass methods like introducing nanofillers [8], incorporating plasticizers [9], employing blending processes [10], or utilizing co-polymerization [11] to improve their performance. Due to its ease of preparation and the dual role of forming new complexation sites between the polymer blend and the ionic dopant, ultimately leading to improved ionic conduction, the blend approach is a favorite among researchers [12–14]. Natural biopolymers, such as CS and PS, stand out for their cost-effectiveness, offering environmentally friendly alternatives with considerable economic advantages. Their abundance and versatility make them attractive choices for various applications, providing a sustainable and affordable solution in material science. Our previous study combined CS with PS and introduced doping with either KSCN or NH$_4$SCN [15, 16]. Our investigations revealed that this polymer blend system, composed of both CS and PS, displayed substantially superior ionic conduction properties when contrasted with individual polymers and other polymer blends frequently utilized as electrolyte systems [17, 18]. This improvement can be attributed to hydroxyl (−OH) and amine (−NH$_2$) groups in the polymer chain. These groups simplify the conduction pathway and, when combined with an ionic dopant, increase σ.

Polymer blending and incorporating nano-fillers are essential in elevating the structural, dielectric, and σ of polymer-based electrolyte systems. For blending, previous studies have demonstrated noteworthy advancements. For instance, the blending of polyvinyl alcohol/polyvinyl pyrrolidone (PVA/PVP) with Li$^+$ incorporation exhibited improved conductivity properties, rendering it suitable for battery applications [19]. Another study explored carboxymethyl cellulose/polypyrrole (CMC/PPy) blends with varying PPy concentrations, showcasing their promise as cost-effective blends with excellent chemical and physical characteristics for energy storage devices [20]. Incorporating nano-fillers further enhances the performance of these electrolyte systems. In previous studies, gold nanoparticles (Au-NPs) and TiO$_2$ nanoparticles were introduced into a (PVP/PVA/CMC) blend, creating novel nanocomposites with exceptional capacitive behavior [21, 22]. Another investigation successfully incorporated graphene nanoplatelets (GNP) and copper nanoparticles (Cu NPs) into polystyrene (PS), resulting in significantly improved charge/capacitive storage abilities for the prepared nanocomposites [23].

Including plasticizers is a straightforward but crucial method to enhance the conductivity of complexes produced by polymer blends and ionic dopants. Plasticizers such as glycerol [24], dimethylacetamide (DMA) [25], tetra (ethylene glycol) dimethyl ether (TDE) [26], propylene carbonate (PC) [27], and ethylene carbonate (EC) [28] are known nonvolatile organic solvents and low molecular weight polymers that have proven successful in external methods. In a previous study, Chai and Isa plasticized CMC doped with oleic acid with glycerol to increase its conductivity to 1.64×10^{-4} S/cm [29]. Similarly, YM Yusof, and M.F.Z. Kadir used glycerol as a plasticizer in blending methylcellulose (MC)-PS doped with LiClO$_4$, achieving higher σ at 4.25×10^{-5} S/cm [30]. Another study by Shukur et al., focused on CS-starch blended biopolymer electrolytes, enhancing σ to 1.02×10^{-4} S/cm by adding EC and using NH$_4$NO$_3$ as the ionic dopant [31]. In a separate effort, DC Dragunski, and A Pawlicka used starch polymers with glycerol (30% of starch mass) as plasticizers, resulting in a conductivity value of 5.05×10^{-5} S/cm [32]. These findings demonstrate that plasticization is a highly promising approach for enhancing the σ of polymer complexes, with optimization achieving values ranging from approximately 10^{-4} to near 10^{-3} S/cm.

Despite extensive research in polymer electrolytes, there is a gap in a suitable model for describing the ionic conduction mechanism. This is primarily due to the focus on enhancing σ and the challenges associated with understanding ion conduction, especially with varying conductivity values. The demand for PE systems with exceptional σ is crucial for efficient charge carrier transport in electrochemical devices. These charge carriers include both anions and cations, with anions typically exhibiting lower charge transport capabilities due to their bulkier nature. To bridge this gap, numerous well-documented approaches have been employed

to assess transport properties, such as FTIR deconvolution [9], Broadband Dielectric Response (BDR) [33], Rice and Roth models [34], Trukhan model [35], and Nyquist fitting [36], all of which contribute to our comprehension of the electrolyte's conduction characteristics. Bandara and colleagues [33] extensively explored the BDR method and found that it's only suitable for Nyquist plots featuring a combination of semicircles and spikes. On the other hand, the Rice and Roth method is particularly effective when dealing with Arrhenius-type behavior. Still, it can sometimes provide questionable results when assessing the transport properties of PEs [36]. When considering transport property parameters, the Trukhan method assigns substantial significance to the characteristics of loss tangent (tan δ) peaks, including their shape and intensity. These tan δ peaks are associated with relaxing dipoles and are typically found in regions of low σ [6].

This study aims to synthesize innovative biopolymer-based electrolyte systems, which have been unexplored so far, to enhance our understanding of the physicochemical properties and impedance response governing the role of glycerol as a plasticizer. The objective is to increase the conductivity and ion transport capability of a polymer blend electrolyte (PBE). Our research specifically explores the influence of glycerol addition on the molecular properties and phase transitions within the PBE. Additionally, we analyze ion transport and conductivity properties using electric equivalent circuit modeling, providing valuable insights into the field. Our approach enhances comprehension of relationships assessed through impedance spectroscopy in solid polymer electrolyte (SPE) systems. This contributes to designing polymer blends with CS and PS, utilizing environmentally friendly and cost-effective materials for improved properties. These blends hold promise for next-generation electrochemical devices. The research aims to develop a new biodegradable electrolyte from natural sources, particularly for electrolyte systems. The ultimate goal is to employ this newly synthesized eco-friendly electrolyte in energy storage devices, such as electric double-layer capacitors (EDLC), which the literature has not examined.

Methodology

Reagents

To prepare for CSPS, we employed a blend of biopolymers consisting of 40% soluble starch from potatoes (PS) [($C_6H_{10}O_5$)n], and 60% CS, which is 60% deacetylated chitin with a molecular weight ranging from 310,000 to 375,000 Da and a viscosity of 800–2000 cP. As the source of ions, we selected lithium perchlorate ($LiClO_4$) in its ACS reagent-grade form, characterized by a purity of 99% and a molecular

weight of 106.39 g/mol. Glycerol, with a molecular weight of 92.09 g/mol, served as our chosen plasticizer, and we incorporated it at concentrations of 11%, 22%, 33%, 44%, and 55%. To formulate the solvent, we utilized a mixture of deionized water and 1% acetic acid (glacial, purity ≥ 99.7%, molecular weight: 60.05 g/mol). In the electrode preparation for electrical double-layer capacitors (EDLC), we employed a blend of carbon black (CB) and activated carbon (AC) sourced from Alfa Aesar. Furthermore, we used polyvinylidene fluoride (PVdF) and N-methyl pyrrolidone (NMP) from Merck as our binder and solvent, respectively. The PVdF employed was in an anhydrous form, boasting a purity level of 99.5% and a molecular weight of 99.13 g/mol.

Synthesis of CSPS film (CSPS-LiCl$_4$-Gly)

The synthesis of CSPS was carried out using a simple solution casting method, following the procedure described below. Initially, 0.6 g of CS, constituting 60% by weight, was dissolved in a 70 mL solution of highly diluted acetic acid (1% concentration) with continuous stirring for a period of 24 h. At the same time, a similar solution was heated to 95 °C and stirred continuously for 1 h to dissolve 0.4 g of soluble starch (PS), accounting for 40% of the total weight. An essential aspect of this process was the precise combination of these proportions of CS and PS biopolymers in the presence of acetic acid as a solvent. According to the references [37, 38], this particular blend was found to be crucial for improving ion transport through the host matrix. In the dissolution process of the polymers (CS and PS) 1% acetic acid was added to distill water, which created a highly diluted (acetic acid + distill water) solvent to facilitate the dissolution process by reducing the PH of the solvent (PH = 5). In addition, the acetic acid solution aids in breaking the strong hydrogen bonds in CS, promoting its dissolution and enhancing its conductivity by increasing bond rotation and segmental motion of chain and side groups. Following this, the two solutions were merged, and 40 wt% of $LiClO_4$ dopant salt was incorporated into the mixture, with continuous stirring sustained for 24 h. Afterward, different concentrations of glycerol were introduced into the mixture and stirred for an additional 20 h. Indeed, in the preceding work [37], the optimal blending ratio for two polymers was initially established, focusing on a high amorphous region. This ratio was then utilized, and varying weight percentages of salt were systematically added to the polymer blend to achieve the best ion-conducting system. Subsequent to these experiments, the PBE with a fixed amount of dopant salt, exhibiting the highest measured conductivity using an LCR meter, was carefully selected. In this investigation, relying on the aforementioned knowledge, the impact of glycerol on the ionic conductivity of polymer electrolytes was explored by altering its concentration in the prepared samples to

Table 1 Arrangement and example code snippets for the CSPS film preparations

CS:PS:LiClO$_4$ (wt%)	Glycerol (wt%)	Designation
60:40:40	11	CPLCG1
60:40:40	22	CPLCG2
60:40:40	33	CPLCG3
60:40:40	44	CPLCG4
60:40:40	55	CPLCG5

further augment the system's conductivity. Table 1 lists the characteristics of the synthesized films and their corresponding designations.

Samples were put into labeled Petri dishes and air-dried for 14 days in a room with a relative humidity of 15%. A desiccator with silica gel inside was also used to dry the samples completely. These films can be used for the characterization and fabrication of EDLC. A digital micrometer was used to measure the thickness of the film. The main stages of the solution casting process for preparing CSPS based films are shown graphically in Fig. 1.

Instrumentation and Characterization of CSPS

Examinations of Structure and Composition

FTIR spectroscopy was performed at room temperature conditions using the transmittance mode. This method involves amplifying and digitizing weak signals from the sample to display a well-defined signal on a screen. The analysis was performed using the "Spotlight 400 Perkin Elmer" spectrometer, which covered the wavenumber range from 400 to 4000 cm^{-1} with a resolution of 1 cm^{-1}. Throughout the examination, specific peaks in the spectra were discerned and grouped into various functional groups (FGs) and vibrational modes.

Electrical Conductivity Characteristics

Electrochemical impedance spectroscopy (EIS) was used to inspect the electrochemical and σ properties of CSPS membranes in a frequency range of 100 Hz to 2 MHz. A compression spring mechanism ensured the connection between the sample holder and the electrolyte was tight. To avoid possible damage to the sample during the test, a potential amplitude of only 10 mV was chosen, and the LCR meter was connected to a computer for data acquisition. The following formula, as referenced in [39], was applied to calculate the electrical conductivity (σ):
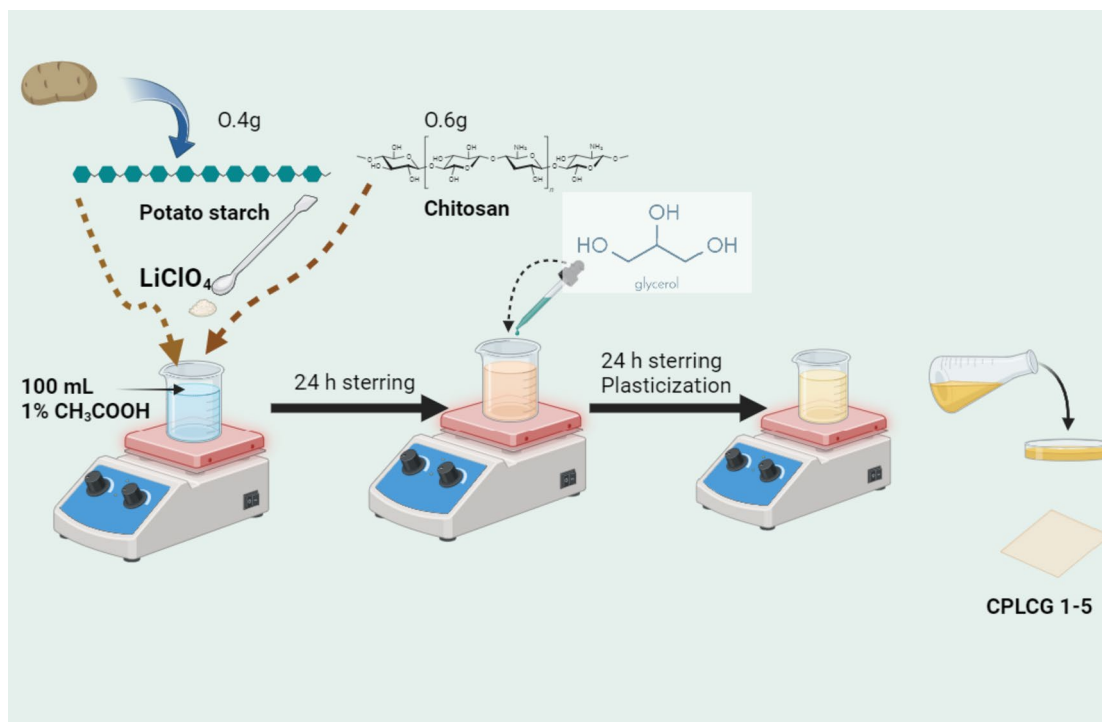
Fig. 1 Basic synthetic steps of CSPS films

$$\sigma = \frac{B}{S \times R_b} \tag{1}$$

The formula mentioned above involves the thickness (in cm), represented as (B) and (S) signifies the area (in cm^2) of the membranes. To ascertain the bulk electrolyte resistance (R_b), we examined the Nyquist plot, plotting the real part (Z_r) against the imaginary part (Z_i). The point at which the line intersected the x-axis, designated as Z_r, held significance for our analysis. The calculation of the real (ϵ') and imaginary (ϵ'')parts of permittivity (ϵ^*) and modulus (M^*) was done using the resulting relations: the real (Z_r) and imaginary (Z_i) parts of the complex impedance (Z^*) [10, 28],

$$Z^* = Z_r - jZ_i \tag{2}$$

$$\epsilon^* = \epsilon' - j\epsilon'' \tag{3}$$

$$M^* = \frac{1}{\epsilon^*} = j\omega C_o Z^* = M' + jM'' \tag{4}$$

It is possible to derive the following relationship from Eqs. (2), (3), and (4) [30, 37].

$$\epsilon' = \frac{Z_i}{\left(Z_r^2 + Z_i^2\right)C_o\omega} \tag{5}$$

$$\epsilon'' = \frac{Z_r}{\left(Z_r^2 + Z_i^2\right)C_o\omega} \tag{6}$$

$$\tan\delta = \frac{\epsilon''}{\epsilon'} \tag{7}$$

$$M' = \frac{\epsilon'}{\epsilon'^2 + \epsilon''^2} = Z_i C_o \omega \tag{8}$$

$$M'' = \frac{\epsilon''}{\epsilon'^2 + \epsilon''^2} = Z_r C_o \omega \tag{9}$$

C_o is the vacuum capacitance in this case and is calculated as $\epsilon_o A/t$, where t is the film thickness and A is the film area. The frequency of the applied field, f, is equal to $\omega = 2\pi f$, which is the angular frequency.

Measurement of Potential Stability and Carrier Transfer

Linear sweep voltammetry (LSV) was used to establish the potential range that is safe for application, and transference number measurements (TNM) were used to determine which charge carrier dominates the membrane. In conducting both LSV and TNM investigations, we employed an identical cell configuration, which involved positioning the CSPS based film between two stainless steel (SS) electrodes. To secure

and optimize electrode contact, a compressed spring mechanism was employed.

In the LSV experiments carried out in this research, we employed a Digi-IVY DY2300 potentiostat manufactured by the V & A instrument brand (Shanghai, China), which was equipped with DY2300 Series software. The LSV test was conducted within a 4 V potential range at a scan rate of 0.01 V per second.

To calculate the ionic transference number (t_{ion}) in the TNM study, we monitored the recorded current over time. The remaining value, denoted as ($1 - t_{ion}$), corresponds to the electronic transference number ($t_{electron}$). Following Wagner's polarization method, we applied a constant DC voltage of 0.2 V across the SS /CSPS film/ SS cell during this test. To measure the current, we used a UT803 True RMS multimeter connected to a computer for data acquisition. Also, the digital power supply was a V & A Instrument DP 3003 DC source. By determining the initial current (I_i) and the steady-state current (I_s) during the measurement, we estimated both t_{ion} and $t_{electron}$ values using the following equations [15]:

$$t_{ion} = \frac{I_i - I_s}{I_i} \tag{10}$$

$$t_{electron} = 1 - t_{ion} \tag{11}$$

Electrode Preparation and EDLC Assembling

Before the assembly of the EDLC, a specific preparation process was carried out on the AC electrodes. Initially, 3.25 g of activated carbon (AC) were dry-milled with 0.25 g of conductive CB. This milling procedure lasted 25 min within a SS jar containing 6 steel balls with a 10-millimeter diameter. A vertical planetary ball mill was used to rotate the jar at a speed of 500 rpm. Then, 15 milliliters of NMP solvent was used to dissolve the carbonaceous material collected in the previous step. A binder of 0.5 g of PVdF was then added to the mixture. This blend was continuously stirred for a duration of 5 h until it reached a dense and evenly distributed black slurry. To create uniform electrodes, this slurry electrode material was applied onto an aluminum foil (AF) using the doctor blading technique, as illustrated in Fig. 2. Afterward, a drying process was conducted for 24 h in a drying cabinet set at 60 degrees Celsius. Finally, the sheet of electrode material was cut into circular shapes with a diameter of 1.6 centimeters to fit perfectly into CR2032 coin cells. These electrode discs had a thickness of 0.025 centimeters and contained approximately 0.00243 g of activated carbon. The mass of the active material was determined by weighing the AF substrate both before and after the coating process.

To construct the EDLC device, the most optimal ion-conducting film, based on its σ and potential stability, was

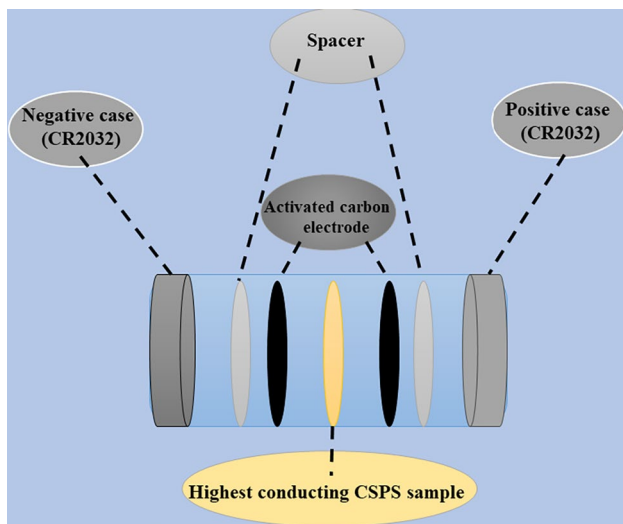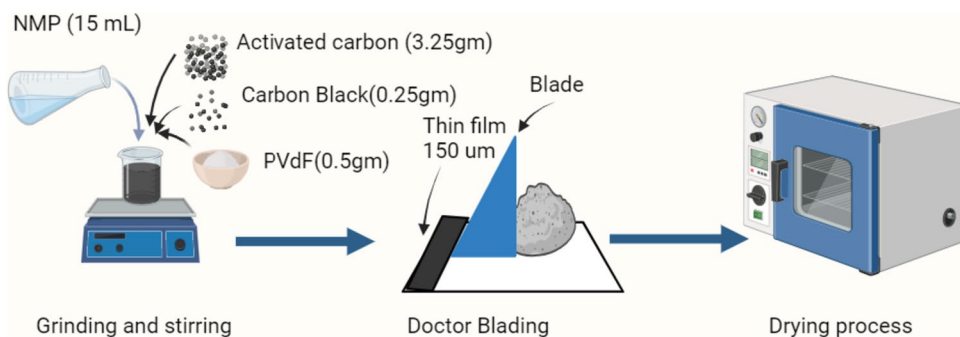Fig. 2 Procedure of AC electrode preparation

Fig. 3 The constituents of the constructed coin cell EDLC apparatus

positioned between two previously prepared circular AC electrodes. In the assembly of the EDLC, spacers were utilized to establish flawless connections and eliminate any gaps within the device. Subsequently, the lower and upper caps of the CR2032 coin cell were utilized to encase the EDLC device. Figure 3 provides a visual representation of the key components involved in the fabrication of the EDLC device.

EDLC Performance Characterization

The same potentiostat that was utilized for the LSV technique was also employed for conducting cyclic voltammetry (CV) measurements in this study. The CV measurements were carried out within a voltage range of 0 to 1 V, employing various sweep rates, namely 20, 50, and 100 millivolts per second (mV S^{-1}), in order to assess the performance of the manufactured EDLC device. The data acquired through these techniques provided sufficient information to evaluate the overall performance of the device and determine the necessary parameters. Specifically, from the CV test, one could

calculate the specific capacitance (C_{spc}) using the formula described in the references [40, 41].

$$C_{spc} = \int_{V_1}^{V_2} \frac{IdV}{2mz\,\Delta V} \tag{12}$$

In these formulas, (z) represents the scan rate for the applied potential, which spans from 0 (V_1) to 1 V (V_2), and (m) corresponds to the mass of the activated carbon (AC). The area of the cyclic voltammetry (CV) curve is extracted using Origin Lab 9.1 software.

Results and Discussion

FTIR Study

Fourier-Transform Infrared Spectroscopy (FTIR) is a highly valuable tool in the research and development of PEs due to its impressive sensitivity and non-destructive nature. This technique employs infrared (IR) radiation to stimulate the vibrations of chemical bonds, allowing for the detection of distinct spectral patterns associated with them. In our study, we conducted FTIR spectroscopy on all CSPS films, as portrayed in Fig. 4. We anticipated that complex interactions would occur between CS and PS, both rich in FGs, and the ionic components of the LiClO$_4$ dopant salt, as well as glycerol with its multiple reactive hydroxyl groups. Our assessment involved observing alterations in the intensity and position of specific spectral bands and the emergence or disappearance of certain additional peaks to gain insights into these interactions [42]. The power of adding a dopant salt and increasing the glycerol content is readily apparent in Fig. 4, particularly in peak position shifts and variations in intensity. For instance, the axial O–H and stretching C–H bands are present in both the pure CS and PS spectra at wavenumbers of 3259.40 and 2924.31 cm^{-1}, respectively [25].

However, with the inclusion of 40% by weight of the dopant salt and 11% by weight of the plasticizer, a distinct shift in the positions of these peaks is observed,

Fig. 4 FTIR spectra over 400–4000 wavenumber range for **a** pure CSPS-Glycerol, **b** CPLCG1, **c** CPLCG2, **d** CPLCG3, **e** CPLCG4 and **f** CPLCG5 films
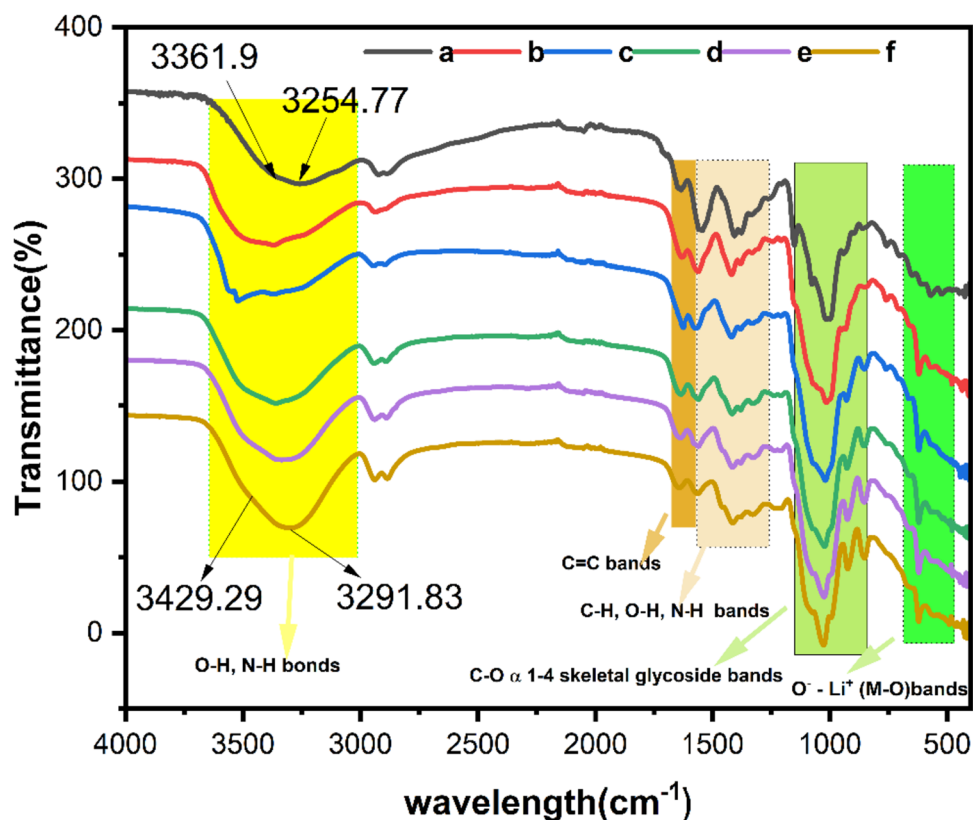
moving to 3352.1 cm^{-1} and 2929.17 cm^{-1}, accompanied by an increase in their intensities. The increased intensity of the O–H (hydroxyl) band compared to other bands can be attributed to the presence of strong hydrogen bonding within and between molecules. Furthermore, increasing the concentration of the plasticizer reinforces the dominance of this particular band. This effect is particularly pronounced because glycerol, which is used as the plasticizer, contains a substantial number of hydroxyl FGs. These hydroxyl groups readily engage in hydrogen bonding interactions, making the O–H band more prominent in the spectrum. In the LiClO$_4$ spectra, the primary fingerprint peak associated with the linear anion vibration group (O$^-$–Li$^+$(M–O)) undergoes a noticeable change as the glycerol content increases. Specifically, this peak shifts to higher wavenumbers, transitioning from 615.11 to 619.97 cm^{-1}, and experiences a significant decrease in intensity. This shift and reduction in the intensity of the O$^-$–Li$^+$(M–O) band has been observed previously in polymer blends containing metal salt systems when the glycerol concentration is increased [43]. Several groups of specific bands, including those containing N-H, O-H, C-H, and C=N functionalities in the range of approximately 1330.50–1640.61 cm^{-1}, show notable changes in terms of their intensities and peak positions due to the addition of glycerol.

Furthermore, the α 1–4 skeletal glycoside bands, which are characteristic peaks of pure polyvinyl alcohol (PS),

exhibit a shift in their positions. For instance, the peak that was initially observed at 1008.48 cm^{-1} for the CPLCG1 sample (Fig. 4b) has shifted to 1023.05 cm^{-1} for the CPLCG5 sample (Fig. 4f). These alterations in the positions and intensities of specific bands serve as compelling evidence of interactions between the FGs of CS and PS and other electrolyte components, including the ions from LiClO$_4$ salt and the glycerol plasticizer. This complexation process creates additional space, facilitating bond rotation and movement of chain segments. As a result, it opens up alternative kinetic pathways within the CSPS host blend, allowing for improved transfer and enhanced mobility of cations, specifically lithium ions (Li$^+$) [42]. One potential conduction mechanism identified in this context is the Grothhus phenomenon, known as structure diffusion (Fig. 5). This mechanism involves the movement of Li$^+$ ions between complex sites within the biopolymer blend. When an electric field is applied, dissociated Li$^+$ ions traverse from one coordination point in the CSPS host to the next through a hopping process, driven by their weak electrostatic interactions with the coordination sites of the host medium [44]. At very high concentrations of glycerol (55 wt%), as depicted in Fig. 4f, the FTIR pattern closely resembles that of pure glycerol, exhibiting maximal hydroxyl peak strength. This corresponds to the multiple hydroxyl components in glycerol's structure, which in turn creates alternative pathways for the movement of mobile ions [16]. The strong interconnection
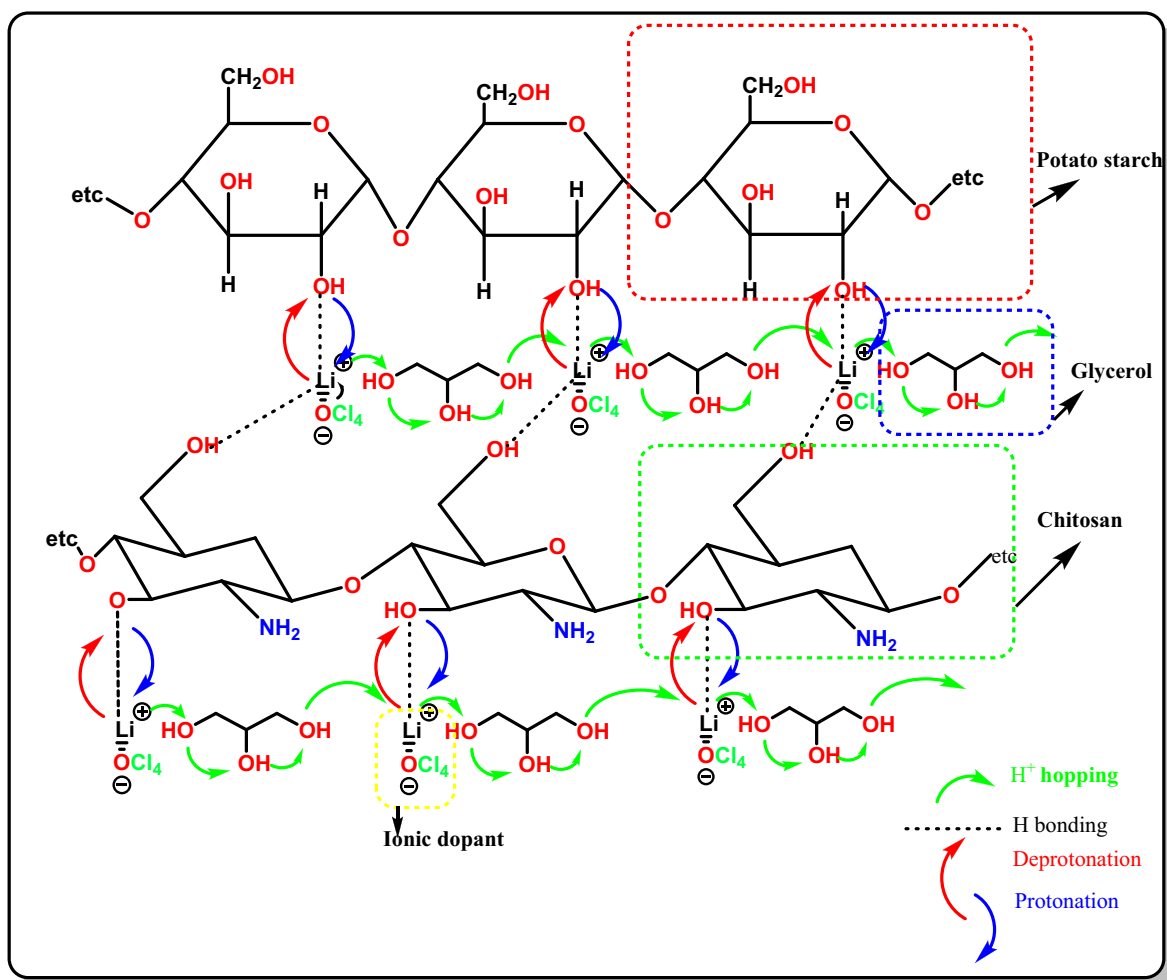
Fig. 5 Proposed Schematic Illustration of Proton (H$^+$) Hopping and Lithium Ion (Li+) Mobility Mechanism in CSPE

between the components of the electrolyte results in a more pliable and less ordered structure.

FTIR deconvolution is a valuable tool in the context of conductivity analysis, offering several advantageous qualities such as improved peak resolution, noise reduction, and the ability to investigate interconnections among deconvolution parameters. This method is particularly useful when assessing conductivity [42]. When employing FTIR deconvolution, it becomes possible to determine the ion fraction responsible for conducting electricity. As noted by Ramelli et al., the deconvolution of FTIR spectra allows for the isolation and manipulation of existing peaks, including adjustments to both their intensity and wavenumber [45]. The appearance of a peak within the 600 to 650 cm^{-1} range, attributed to ClO$_4$, is a commonly employed indicator for investigating ion-ion interactions in PE when incorporating LiClO$_4$ salt [43, 44]. The ClO$_4$ bands display two discernible peaks spanning the 610 to 630 cm^{-1} range, implying the potential existence of up to two different ClO$_4$ anion configurations within this material. Research conducted by Abarna

et al. has previously proposed an association between Li$^+$ ions and the ClO$_4$ band in the 610–630 cm^{-1} range. Furthermore, lower frequencies below 610 cm^{-1}, have shown the presence of CIP ClO$_4^-$ anions, while approximately 610–630 cm^{-1} is indicative of free ClO$_4$ anions [44]. The deconvoluted FTIR spectra of the prepared electrolyte are shown in Fig. 6a–d. From Fig. 6, the peaks of the contact-ion pairs are less pronounced than the peaks of the free ClO$_4$ ions. This observation underscores the role of glycerol plasticizer in facilitating the dissolution of LiClO$_4$ salt within the CS:PS matrix, and this interaction becomes apparent when these two components are combined.

The equations presented in reference [46] were employed to gauge the presence of free ions and contact ion pairs by analyzing the FTIR band areas [16, 36]:

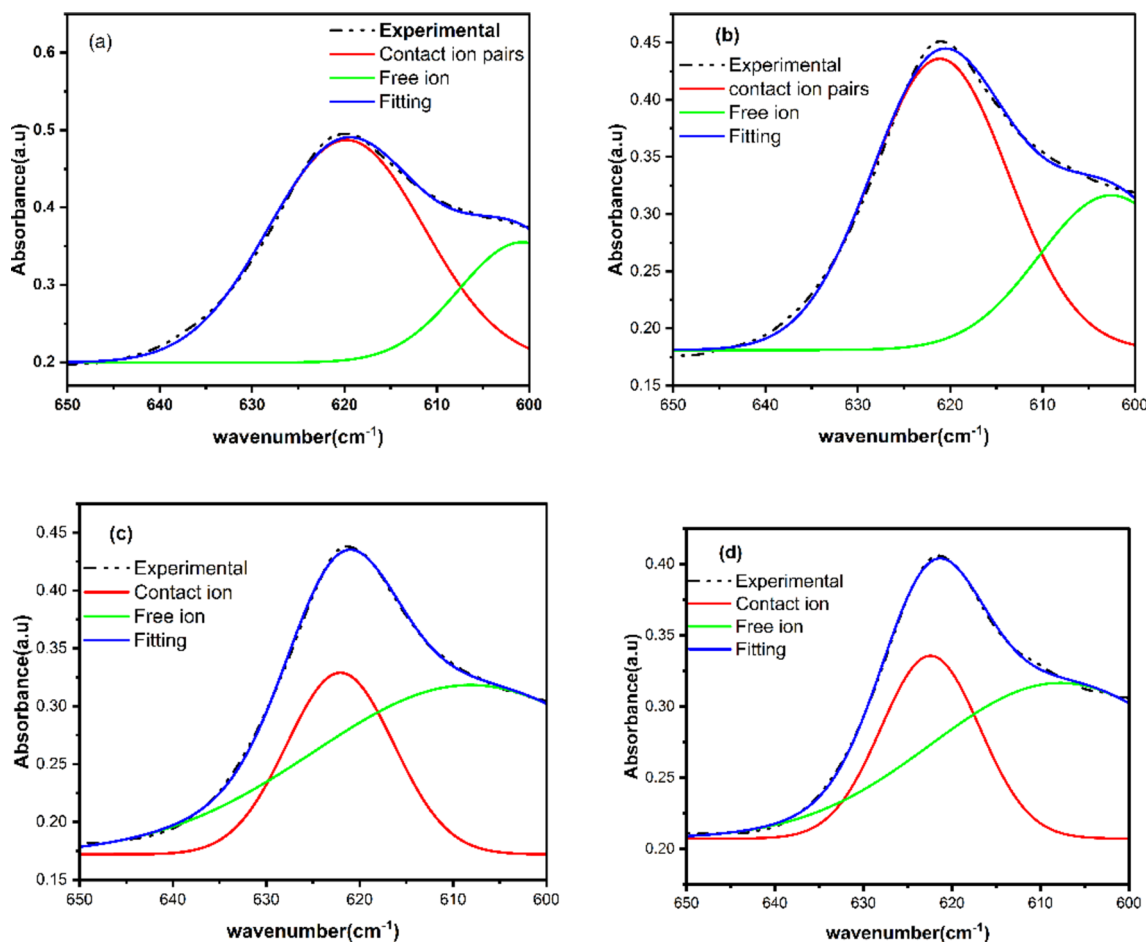$$\text{Percentage of FI } (\%) = \frac{A_f}{A_f + A_c} \times 100\% \qquad (13)$$

Fig. 6 Deconvoluted FTIR spectra for **a** CPLCG2, **b** CPLCG3, **c** CPLCG4 and **d** CPLCG5

Table 2 The percentage areas of free ions and contact ions extracted from Fig. 6 in the wavenumber range of 600–650 cm^{-1}

Sample	FI%	CIP%
CPLCG2	17.3588	69.4508
CPLCG3	35.95992	82.6412
CPLCG4	69.03693	64.04008
CPLCG5	73.18754	26.81246

$$\text{Percentage of CIP (\%)} = \frac{A_c}{A_c + A_f} \times 100\% \tag{14}$$

In Table 2, the percentages of free ions (FI) and contact ion pairs (CIP) are indicated based on the respective areas, where A_f represents the area of FI, and A_c represents the area of CIP.

The elevation in σ can also be linked to the greater abundance of separated Li$^+$ ions originating from LiClO$_4$ salts. A connection between conductivity and the ratio of unbound ions has been confirmed in accordance with the research conducted by Aniskari and collaborators [47].

Electrochemical Investigations

Impedance Study

The impedance technique is a highly effective tool in materials science and electrochemistry, offering researchers valuable insights into the electrical characteristics of materials. Through the application of this method, it becomes feasible to recognize and distinguish among various electrical phenomena occurring at different frequencies. More precisely, the impedance technique offers the capability to identify the relaxation frequency and differentiate between the low-frequency tail and the high-frequency semicircular region, each associated with distinct bulk characteristics of the material being studied. Additionally, when employing EIS, it allows for the determination of the frequency-dependent real and imaginary components of impedance, which are referred to as Z_r and Z_i, respectively. In the field of materials research,

the impedance technique proves to be indispensable for evaluating the DC conductivity [48]. This method involves subjecting an electrochemical sample holder to an alternating current (AC) field at various frequencies, thereby allowing for the calculation of EIS values. By doing so, researchers gain valuable insights into the electrical behavior of these films.

It can be noted from Fig. 7a–e that the inclined line observed in the plot is a result of the charge transfer resistance and capacitance associated with the electric double layer (EDL) formed at the interfaces of electrolyte and electrode, while the semicircle signifies the R_b of the electrolyte membrane [49, 50]. This indicates the partially resistive and capacitive characteristics of the
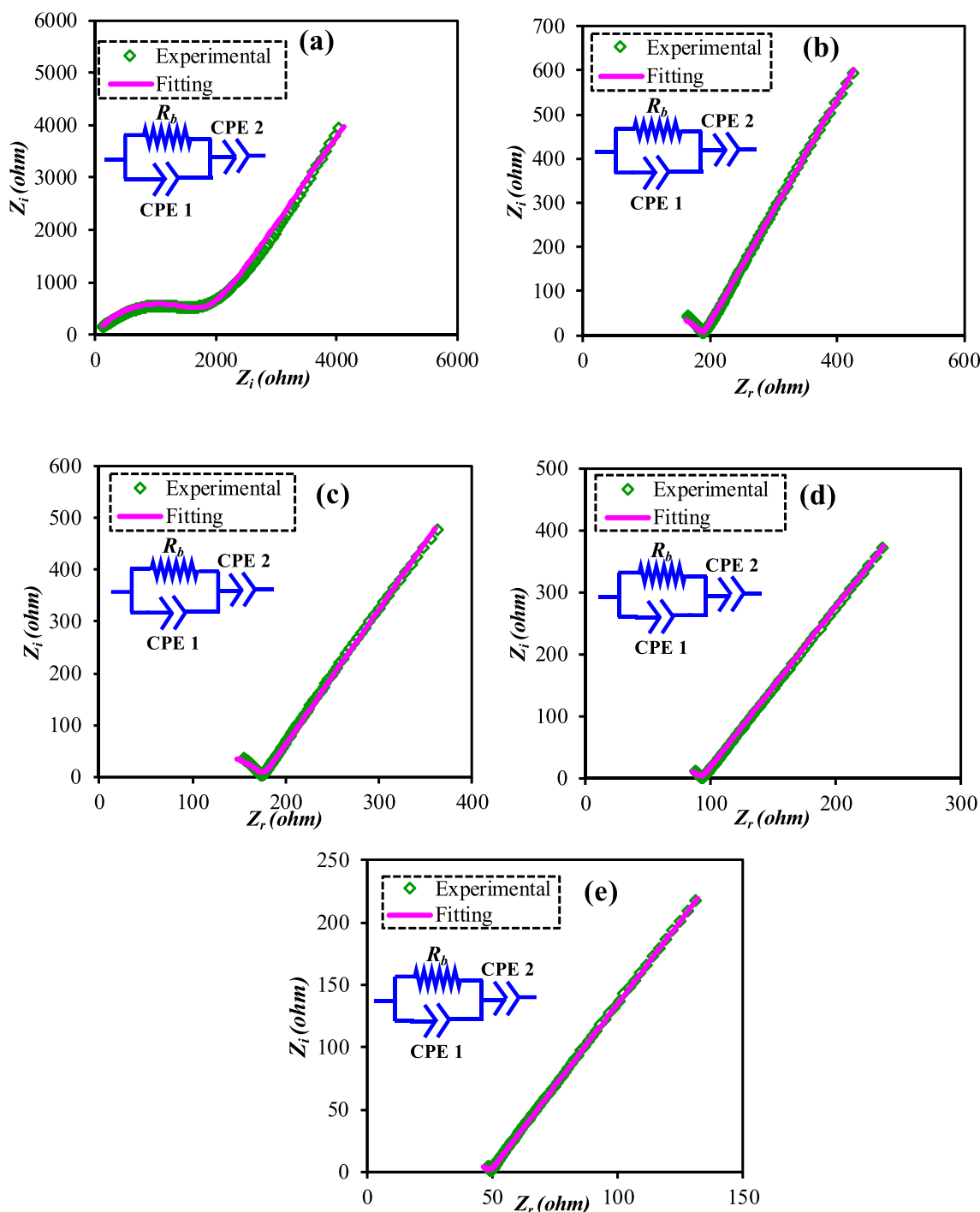

Fig. 7 Impedance plot and EEC modelling for **a** CPLCG1, **b** CPLCG2, **c** CPLCG3, **d** CPLCG4, and **e** CPLCG5

Table 3 The DC value of CS:PS: LiClO$_4$:Glycerol films

Samples	$R_b(\Omega)$	DC conductivity (S/cm)
CPLCG1	1800	5.48×10^{-6}
CPLCG2	189	5.22×10^{-5}
CPLCG3	176	5.61×10^{-5}
CPLCG4	93	1.07×10^{-4}
CPLCG5	49	2.01×10^{-4}

Table 4 Room temperature EEC fitting parameters for all samples

Sample	n_1	n_2	CPE$_1$ (F)	CPE$_2$ (F)
CPLCG1	1.060	1.040	1.43×10^{-8}	2.35×10^{-6}
CPLCG2	1.105	1.195	2.00×10^{-8}	1.15×10^{-5}
CPLCG3	1.110	1.205	2.50×10^{-8}	1.39×10^{-5}
CPLCG4	1.080	1.200	3.33×10^{-8}	1.82×10^{-5}
CPLCG5	1.080	1.210	7.14×10^{-8}	2.99×10^{-5}

sample. Notably, as the concentration of glycerol increases in the prepared samples, the impedance plots exhibit a pronounced spike with a shrunk semicircle portion, indicating their highly capacitive nature. The nearly complete disappearance of semicircle in the largest plasticized samples indicates that ionic transport is facilitated by freely mobile ions, resulting in reduced electrolyte resistance and improved conductivity. To more precisely assess the influence of glycerol on the DC conductivity of the films, Table 3 provides a thorough summary of the collected data with their respective R_b values. A clear enhancement in conductivity value can be noticed reaching the optimum value of 2.01×10^{-4} S/cm for the CPLCG5 sample. The outcomes underscore the significance of glycerol as a plasticizer in enhancing salt dissociation, attributed to its reactive polar hydroxyl groups and substantial $\epsilon\prime$ (42.5) [51]. These properties contribute to reducing ion association and ultimately increasing the number of ion carriers. The incorporation of glycerol additionally enhances the flexibility of the film, facilitating polymer chain segmental motion [50]. The lowered energy barrier for polymer chain movement enabling a greater degree of rotation. This, in turn, facilitates easier ionic transport, leading to improved conductivity [52]. A useful approach in interpreting impedance data is comparing an imagined impedance component with its counterpart using electric equivalent circuit (EEC) modeling [52]. This comparison aids in understanding how the material's electrical properties vary with frequency. The impedance graph typically includes a high-frequency segment, which aligns with a parallel combination of capacitor, usually known as constant phase element (CPE) or a leaky capacitor and resistor, as shown in the inset of Fig. 7, and a spike, which represented by another capacitor in series. The values of the EEC elements and fitting parameters are detailed in Table 4. The CPE values exhibit an increase with higher glycerol content, reaching the maximum magnitude for the largest glycerol content sample. The increased capacitance value is attributed to the greater availability of ions for electrode polarization with an increase in ion concentrations in the electrolyte [53]. The slanted inclination of the spike in the Nyquist plots may be attributed to ion migration and nonhomogeneity at the electrolyte/electrode

interface [50]. The EEC fitting trend demonstrates a close match between practical and fitting data. The mathematical expressions for determining the impedance of the CPE element (Z_{CPE}), Z_r and Z_i associated with the EEC model for the sample displaying both a semicircle and spike shape are as follows [54]:

$$Z_{CPE} = \frac{1}{C\omega^n}e^{-j\frac{\pi}{2}n} = \frac{1}{C\omega^n}\left[\cos\left(\frac{\pi n}{2}\right) - i\sin\left(\frac{\pi n}{2}\right)\right] \quad (15)$$

$$Z_r = \frac{R_b^2(L1) + R_b}{2R_b(L1) + O + 1} + \frac{L2}{C_2\omega^{n_2}} \quad (16)$$

$$Z_i = \frac{R_b^2(L3)}{2R_b(L1) + O + 1} + \frac{L4}{C_2\omega^{n_2}} \quad (17)$$

where

$$L1 = C_1\omega^{n_1}\cos\left(\frac{\pi n_1}{2}\right); O = R_b^2C_1^2\omega^{2n_1}; L2 = \cos\left(\frac{\pi n_2}{2}\right);$$
$$L3 = C_1\omega^{n_1}\sin\left(\frac{\pi n_1}{2}\right); L4 = \sin\left(\frac{\pi n_2}{2}\right)$$

In this context, the n_1 parameter signifies the distortion of the arc shape from the ideal semicircle, indicating the deviation of the arc from the vertical axis. On the other and, n_2 highlights the slope of the spike in the low-frequency region, representing the deviation of the spike from the horizontal axis

Plasticizers are chemical compounds often added to polymer matrices to increase their flexibility and reduce their stiffness. In the context of electrolytes, these polymers are typically solid or semi-solid materials. By incorporating plasticizers, the PE becomes more flexibility, which allows the electrolyte to conform better to the outlines of the electrodes within a supercapacitor or electrochemical cell. This ensures enhanced interaction at the electrolyte and electrode interfaces, ultimately reducing the cell's internal resistance. Plasticizers can improve ionic mobility within the PE by creating spaces or channels between polymer chains. These spaces provide pathways for ions to move

more freely, thus increasing the overall σ of the electrolyte. This improved ion mobility results in better charge and discharge rates for the electrochemical device, making it more efficient. Plasticizers can impact on different parameters like viscosity, thermal stability, and mechanical strength. Engineers and researchers can select plasticizers that best match the requirements of the particular electrochemical device they are designing.

The comparison of DC σ values across various studies highlights the remarkable performance of the plasticized composite SPE films developed in this research. In the current study, it is evident that the film with the lowest R_b value exhibits the highest DC σ. Specifically, the maximum DC σ achieved in the research is an impressive 2.01×10^{-4} S cm^{-1}. This remarkable result was obtained with a glycerol concentration of 55 wt% in the CS:PS: LiClO$_4$ electrolyte system at room temperature (RT), as detailed in Table 3. To provide context, a comparison with previous works in the field is noteworthy. For instance, YK.H. Teoh et al. reported a DC σ of 1.55×10^{-6} S cm^{-1} for the Corn starch: LiClO$_4$:Glycerol system at room temperature [55], and YM Yusof et al. reported a value of 4.25×10^{-5} S cm^{-1} for the Methylcellulose(MC): PS: LiClO$_4$:Glycerol system [30]. Notably, the DC σ achieved in the current research surpasses the values reported in these previous works, indicating the effectiveness of the developed CSPS films. Moreover, other studies have reported similar or comparable DC σ values in biopolymer electrolyte systems. For instance, CW Liew

et al. achieved a DC σ of 1.47×10^{-4} S cm^{-1} for a PE system of Corn starch: LiPF$_6$ with BmImPF$_6$ plasticizer which was applied to a primary supercapacitor [56]. Similarly, KH Teoh et al. reported a DC σ of 1.23×10^{-4} S cm^{-1} for a biopolymer electrolyte system of Corn starch:LiClO$_4$ and applied it to a primary barium titanate [57]. In conclusion, the DC σ achieved in the present research stands out as a noteworthy achievement, surpassing several previous studies in the field and demonstrating the potential of the developed CSPS films for various electrochemical applications.

Electrical Conductivity Study

Figure 8 displays the AC conductivity as a function of frequency at room temperature, providing fascinating insights into the characteristics of materials with differing levels of plasticizer content. This AC conductivity plot illustrates three distinct regions, each with its own characteristics and significance. The initial region, observed at low frequencies, is associated with the phenomenon known as electrode polarization. This region's behavior varies with the addition of plasticizers. Electrode polarization emerges due to the buildup of charges at the interface between the electrode and the electrolyte. The degree of this polarization is impacted by the existence and characteristics of plasticizers within the system. In fact, interfacial polarization and the accumulation of charges in the bulk region are distinct electrical phenomena encountered in materials. Interfacial polarization occurs

Fig. 8 Frequency-dependent real part of CSPS conductivity for different plasticizer concentrations
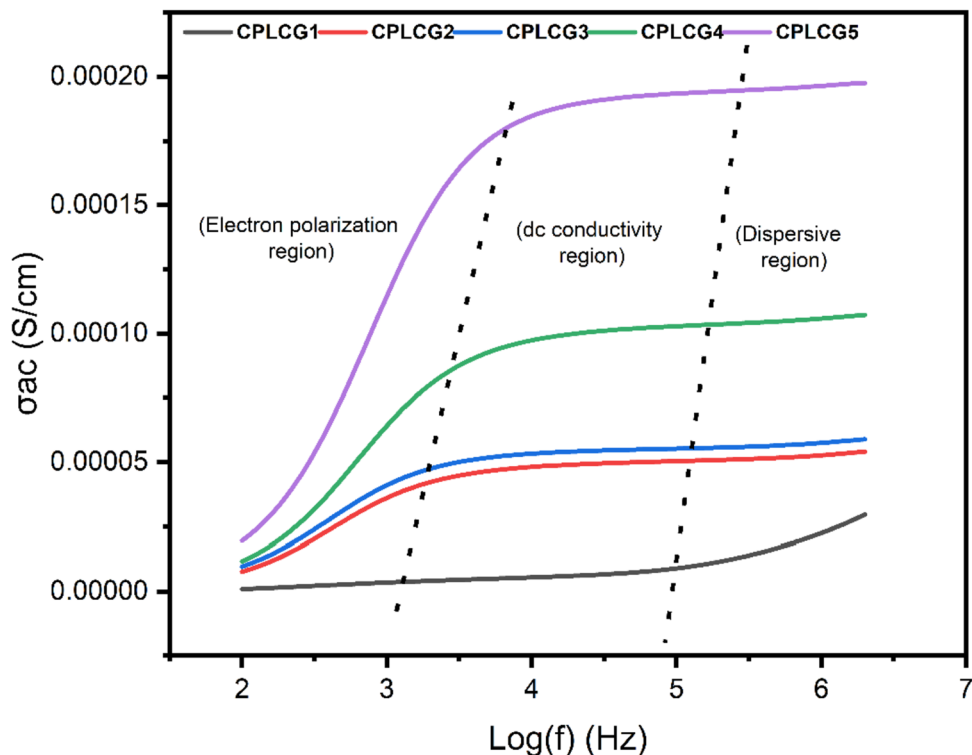
at boundaries between different materials or phases, resulting in the alignment or reorientation of dipoles. This phenomenon is attributed to variations in electric susceptibility or conductivity at interfaces and contributes to the overall dielectric behavior of materials, particularly at interfaces such as those between dielectric materials and electrodes in capacitors. On the other hand, the accumulation of charges in the bulk region involves the presence of excess charges within the volume or bulk of a material. This accumulation can arise due to conductivity, applied electric fields, or external influences, impacting the material's overall conductivity and electrical response. While interfacial polarization predominantly occurs at interfaces, the accumulation of charges in the bulk region primarily takes place within the body of the material, highlighting the different spatial locations and influences of these two phenomena on the electrical properties of materials.

The AC conductivity second section of the graph signifies the intermediate frequency plateau, where long-distance ion movement transpires through a hopping mechanism. It is within this frequency range that the direct current (DC) conductivity is extracted. This plateau-like behavior signifies relatively stable ion transport, and the conductivity measured in this region provides valuable information about the material's ability to support ion conduction [58]. The third segment in the AC conductivity diagram is marked by frequency dispersion. This phenomenon is linked to a heightened likelihood of ions moving from one location to another through hopping. Improved conductivity values in this range indicate an increased hopping frequency. In the high-frequency spectrum, two processes are in action: correlated forward-backward-forward migration (where ions may return to their original position), and successful hopping when the hopping frequency (wh) surpasses a critical threshold (Wh). This transition denotes the stage at which ions effectively jump to new locations as a result of relaxation, leading to an enhancement in conductivity [59, 60].

Dielectric Spectroscopy Study

The observed trends in both the ϵ' and ϵ'' offer valuable insights into the electrical characteristics of the investigated SPEs. Understanding these frequency-dependent changes is crucial for optimizing and tailoring these materials for various applications, such as in batteries, capacitors, and other electrochemical devices. Figures 9 and 10 present a comprehensive view of the frequency-dependent behavior of all SPEs of CSPS blend. These plots reveal a consistent pattern observed across all the samples, characterized by a decrease in the ϵ' and ϵ'' as the frequency increases. In the low-frequency range, a notable feature is the high ϵ' observed. This occurrence can be ascribed to the prevalence of electrode polarization phenomena. Electrode polarization occurs when charges a mass or ions become fixed at the junction

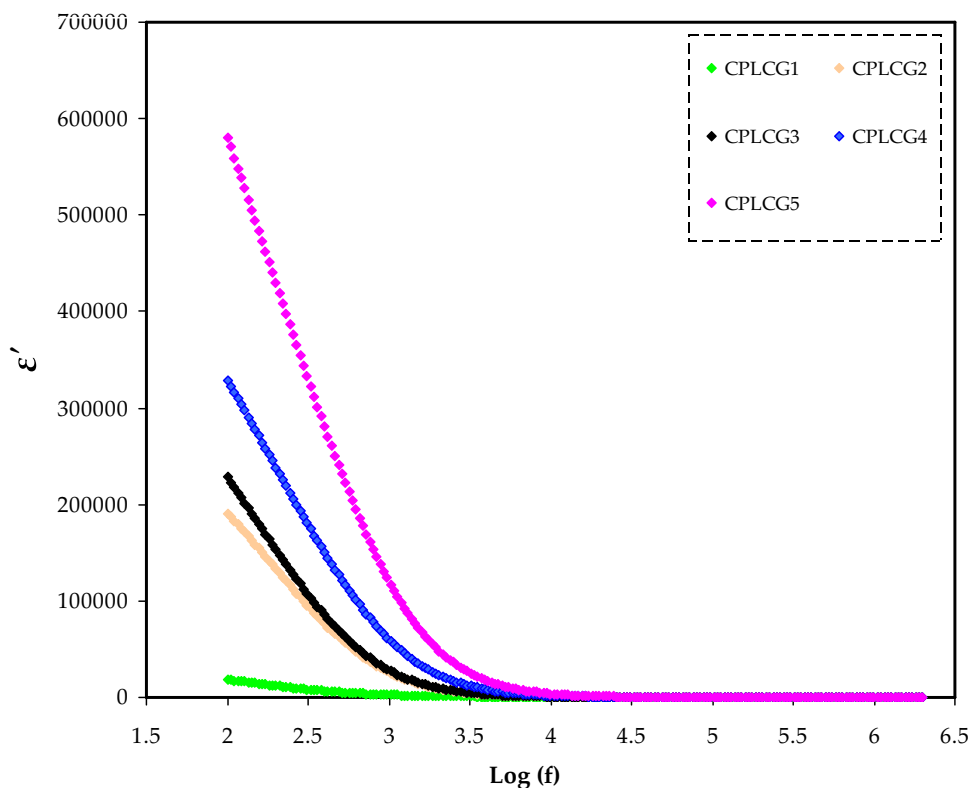Fig. 9 The spectra of ϵ' vs. log (f) for all prepared films

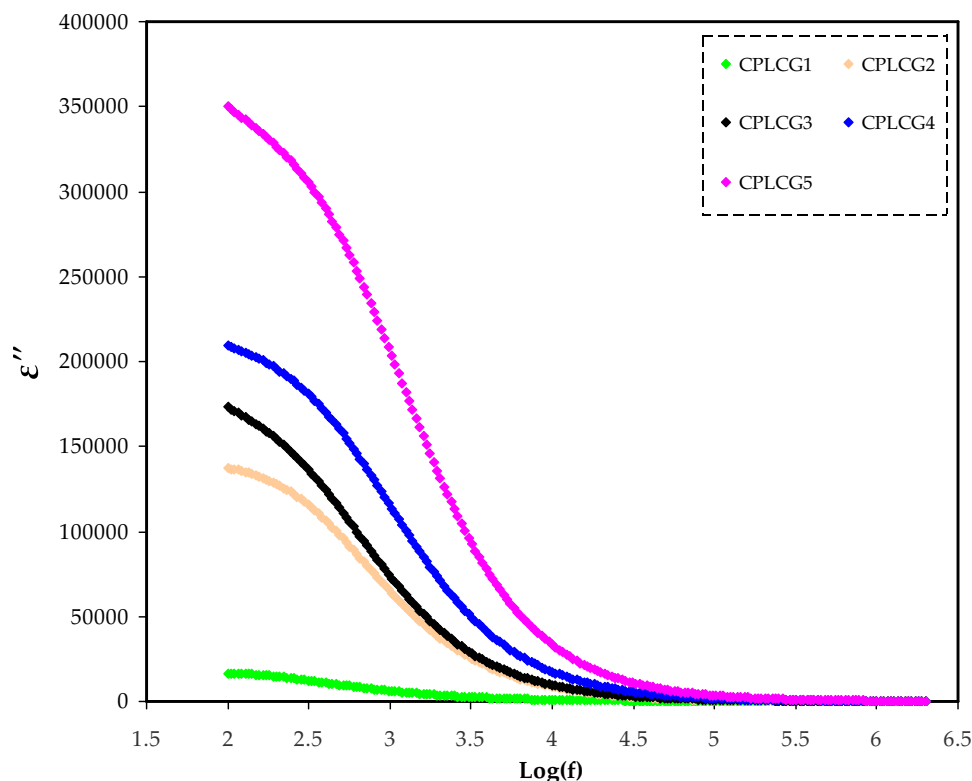**Fig. 10** The spectra of ε'' vs. log (f) for all prepared films

Table 5 Dielectric constants for all the prepared samples at 10^5 Hz at room temperature

Sample designation	Dielectric constant (ε')
CPLCG1	29.9
CPLCG2	30.5
CPLCG3	52.2
CPLCG4	85.0
CPLCG5	112.4

between the electrode and the electrolyte. This accumulation or immobilization results in an elevated ε' in the lower frequency range. With increasing frequency, the influence of electrode polarization gradually diminishes, leading to a corresponding decrease in the ε'. This trend is commonly observed in dielectric spectroscopy and reflects the transition from low-frequency phenomena related to charge accumulation to higher-frequency behavior characterized by more mobile ions within the electrolyte [61]. Both The frequency-dependent behavior of the ε' and ε'' in plasticized systems is illustrated in Figs. 9 and 10. Notably, among all the samples, the system containing 55wt% glycerol exhibits the highest ε' as the values are tabulated in Table 5. The rise in the ε' can be attributed to several factors, including a high concentration of charge carriers and the amorphous nature of

the system. Both the ε' and ε'' exhibit a decreasing trend as the frequency increases. This decrease is particularly rapid at low frequencies, and saturation is observed at high frequencies, as indicated in the figures. This behavior can be attributed to the inability of dipoles within the material to respond quickly to the changing frequency of the applied electric field. The delay between the field frequency and dipole oscillation results in the observed decline in ε' and ε'' with increasing frequency.

The observed variations in dielectric behavior offer valuable insights into the underlying mechanisms. At low frequencies, the high ε' primarily comes from interfacial polarization, while the significant increase in ε'' is a consequence of the movement of free charges within the material. These charges respond to the applied electric field, contributing to the overall dielectric response. At higher frequencies, the ε' remains relatively stable due to the presence of space charge effects near the electrodes, linked to the concentration of charge carriers in close proximity to the electrodes. Nevertheless, these carriers cannot keep up with the periodic reversal of the electric field, resulting in a consistent dielectric response. It is essential to emphasize that the ε' behaves differently in polar and nonpolar materials. In polar polymers, ε' generally demonstrates a higher value and can be affected by factors such as temperature and the inclusion of plasticizers. With the growing concentration of plasticizers in polar materials, there is generally a concurrent elevation in ε'. This uptick is linked to the enhanced

alignment of dipoles and the increased mobility of charge carriers, particularly as the temperature climbs. This behavior is well-documented in the literature and plays a critical role in understanding and optimizing the dielectric properties of materials for various applications [62, 63].

Loss Tangent Study

Figure 11 presents a graphical representation of tan δ plotted against frequency at various plasticizer concentrations. This plot offers valuable insights into the relaxation processes occurring within the material. At lower frequencies, there is a synchronization of the phase between polarization and the electric field, leading to a minimal loss angle or phase deviation. To put it in simpler terms, polarization closely tracks the electric field, resulting in minimal energy dissipation within the dielectric and generating only minimal heat.

However, as the frequency of the applied field increases, polarization progressively lags behind the electric field. This phase shift results in energy dissipation within the dielectric, leading to the generation of heat. When the tan δ reaches its peak, it signifies a resonance condition, indicating that the relaxation time of polarization matches the period of the applied field [64]. Jiang et al. [65] argue that the rise in the tan δ observed as the applied field frequency increases is mainly due to resistive losses. Essentially, mobile charges within the electrolyte layer encounter difficulties in keeping up with electric fields of higher frequencies. Figure 11

further illustrates an increase in tan δ with frequency, reaching a peak value before declining. An interesting observation is that the peak frequency of the maximum tan δ shifts to higher values as the glycerol concentration increases. This shift is attributed to the influence of plasticizers, which lead to an upward displacement of the peak frequencies. This phenomenon suggests that the relaxation time becomes shorter with higher plasticizer concentrations. This behavior aligns with the formula $\sigma = \sigma_o e^{Ea/kT\epsilon'}$, where E_a represents the activation energy. Given that the ϵ' of the electrolyte system is boosted by the presence of plasticizers, it logically pursues that an increase in plasticizer concentrations results in a higher $\epsilon\prime$, subsequently shifting the frequency at which the maximum tan δ is observed to higher frequencies [66].

In Fig. 11, the peak in the tan δ plot refers to the existing relaxing dipoles in all the samples. This relaxation peak shifts toward the high-frequency region with increasing glycerol content, indicating a reduction in relaxation time and highlighting the appearance of rapid segmental relaxation. In fact, with increasing glycerol content, that sample is expected to record a higher value of $\epsilon\prime$ due to two main factors. First, glycerol has a room temperature $\epsilon\prime$ of around 41, which is much higher than that of pure CS and PS [which is around 5]. Second, glycerol has multiple OH FGs that can significantly interact with the FGs of the host polymer blend (CS:PS). This interaction results in intra and interchain molecular hydrogen-bond interruption, enlarging the chain spacing and elongating disordering. This process

Fig. 11 tan δ as a function of log(f) for all the prepared films
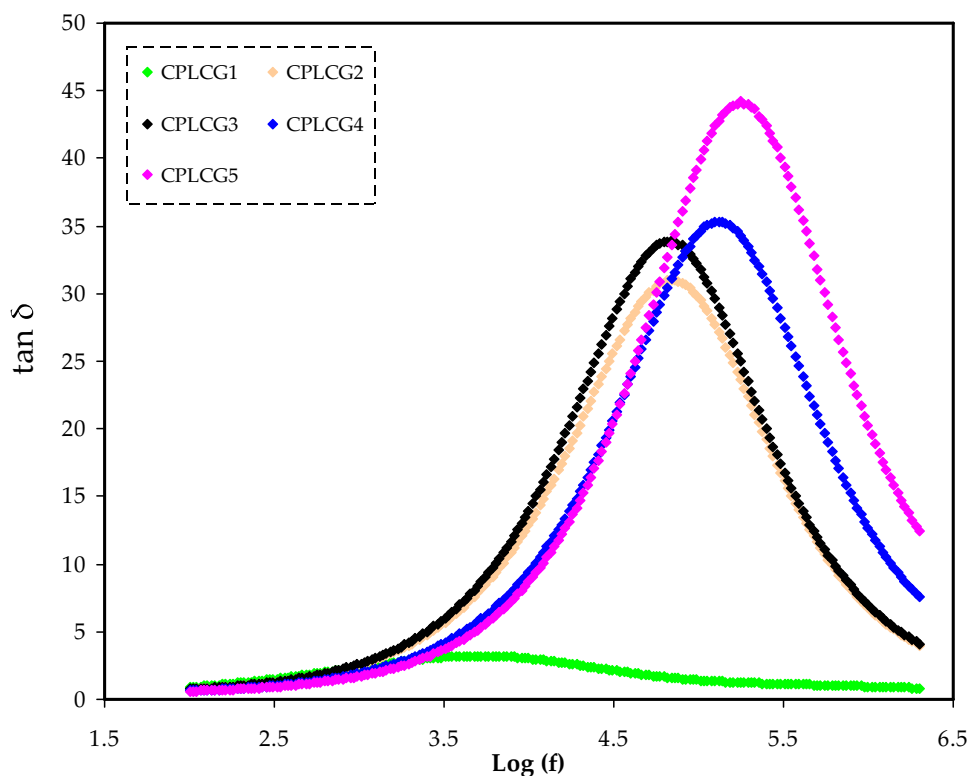
improves the degree of rotation along with expanded inter-chain spacing and more free volume, which is ultimately crucial for an increment in the mobility of cation. According to Debye relaxation process, all dipoles in the system relax with the same relation time, which is called a single relaxation time approximation (Debye behavior) and appears as a single sharp peak in the plot. The single-relaxation-time model of Debye assumes a simple exponential decay of the relaxation function and a single relaxation time for some processes, which typically strongly diverges from the experimental observations in complex systems such as polymers and polymer composites (non- Debye behavior). Here, we have a broad peak (dispersion), which is a sign of the non-Debye relaxation time of the system, which is more expected in the case of polymer-based electrolyte systems. The broadness of the tan δ peaks indicates the attendance of multiple non-Debye-type relaxation processes within the material [67]. These observations highlight the complex interplay between frequency, plasticizer concentration, and the material's dielectric properties, shedding light on the intricate relaxation dynamics occurring within the electrolyte system.

The Electric modulus (M^*) Study

The M^* is a fundamental tool for comprehending the low-frequency bulk relaxation behavior of materials. It serves as a valuable approach to tackle common challenges such as electrode polarization (EP) and conduction effects that might otherwise obscure relaxation when studying dielectric permittivity [68, 69]. Complex impedance data, represented by Z_r and Z_i, are utilized to calculate M' and M'' components of the M^* [69, 70], as described by Eqs. (8) and (9). In

Fig. 12 it becomes evident that at lower frequencies, the M' value approaches zero. The M' spectra exhibit a distinctive pattern contrasted with the ϵ' behavior. As demonstrated in Fig. 13 it showcases the M'' spectra for all the tested samples, particularly at low frequencies, where a high $\epsilon\prime$ value is observed. Recent research has underscored the importance of utilizing the M^* framework to investigate electrical relaxation processes [71]. The traditional exponential Debye model lacks the ability to adequately characterize this relaxation, as evidenced by the asymmetric shape of M''. To gain a thorough insight into the electrical conductivity of polymer electrolytes, it is essential to grasp the involved relationship between the movement of ions and the motion of polymer segments [72–74]. It is noteworthy that an increase in glycerol concentration leads to the shifting of the relaxation peak towards higher frequencies, as depicted in Fig. 14. In the context of a solid electrolyte system involving plasticized CS:PS:LiClO$_4$:glycerol, the relaxation dynamics exhibit characteristics of both viscoelastic relaxation and conductivity relaxation. To investigate the effects of varying plasticizer concentrations on these relaxation mechanisms within the polymer electrolyte, Argand diagram is plotted, as illustrated in Fig. 14.

Figure 14 displays a series of Argand plots corresponding to varying levels of plasticizer. In the figure and its inset, an incomplete half-semicircle is evident, which deviates from the Debye model (i.e., a single relaxation time). This suggests the existence of a range of relaxation times that need to be considered to fully interpret the data. In such scenarios, a greater number of ions and dipoles become engaged in dielectric relaxation. The extensive segmental movements of polymer chains, which involve breaking and reformating

Fig. 12 The graph depicting M' against the logarithm of frequency (log f) for all the plasticized films
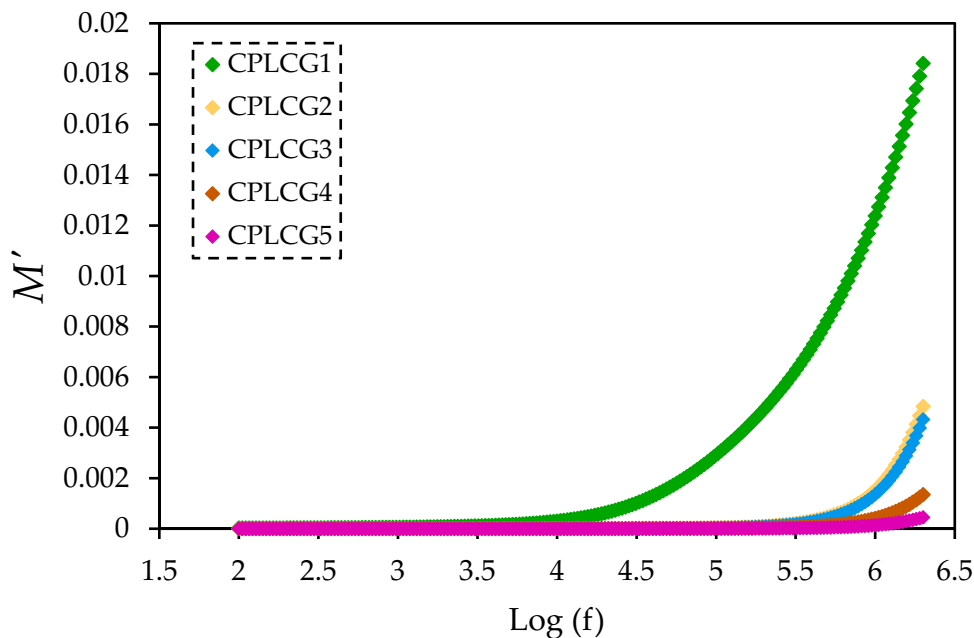
Fig. 13 The graph illustrating M'' as a function of the logarithm of frequency (log f) for all the plasticized films
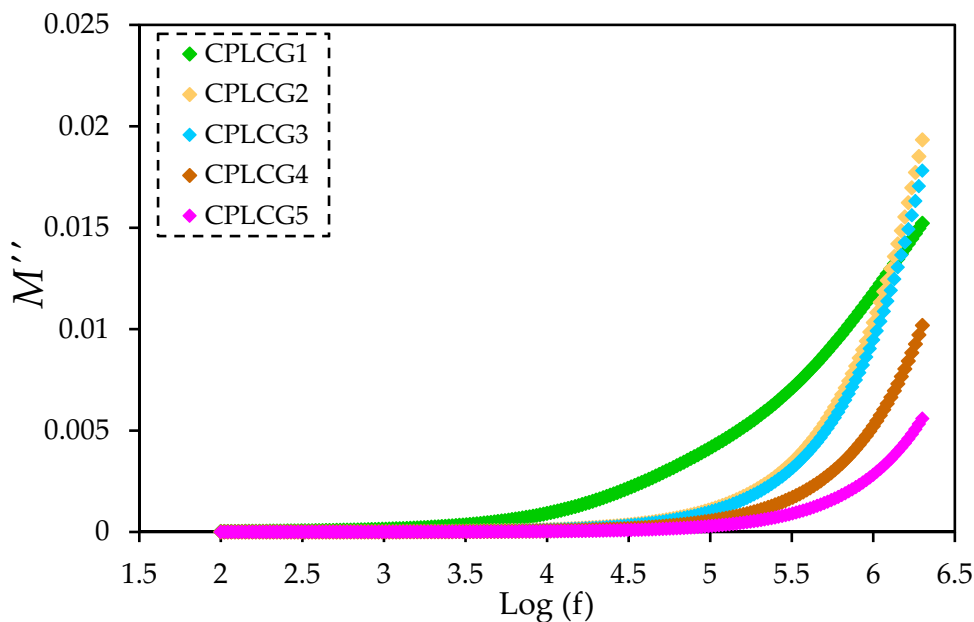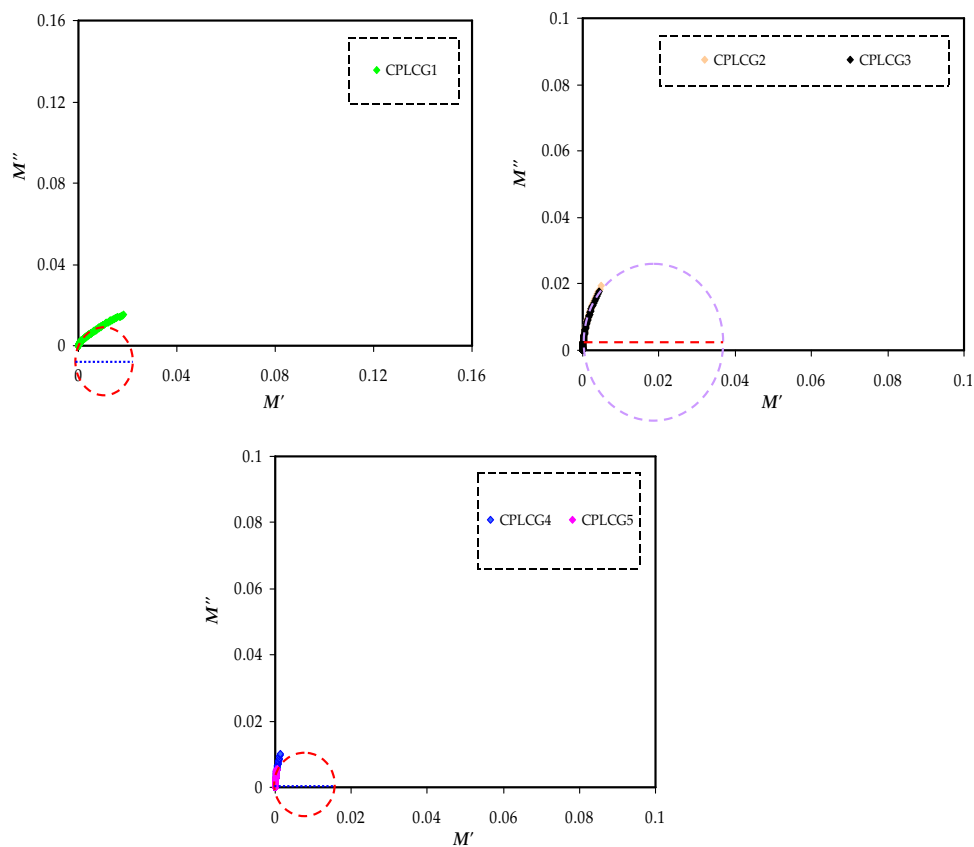

Fig. 14 The M''-M' graph for all the plasticized electrolyte films

coordination bonds crucial for ion transport, contribute to this phenomenon. These movements simultaneously create the necessary free space for cation transport, aiding in the interpretation of the data [75]. Additionally, the incorporation of higher plasticizer concentrations induces a clear shift in the Argand curves, causing them to migrate toward the origin. This transformation can be ascribed to the augmented ionic mobility facilitated by the plasticizers, which, in turn, leads to a decrease in both Z_r and Z_i values, indicative of the amplified conductivity. When the Argand plots (M'' vs. M') exhibit a semicircular shape in the transition from CPLCG4 to CPLCG5, it becomes evident that the relaxation process

is predominantly influenced by the dynamics of conductivity relaxation. This suggests a separation between the motion of ions and the motion of polymer segments [76]. In contrast, the Argand plots provide insight into a distinct viscoelastic relaxation behavior for CPLCG1-3, evident in an incomplete semicircle within the M'' vs. M' plot. Thus, Argand plots serve a crucial role in differentiating the ion transport mechanism in quasi-SPEs, offering insights into the complex mechanisms governing their electrical characteristics.

Electrochemical Analysis

Transference Number Measurement (TNM)

TNM is a valuable methodology for characterizing the intricate process of ion transport within SPEs. This technique is essential in developing and fine-tuning SPEs for their diverse applications across electrochemical devices. To further assess the viability of CPLCG5, which boasts the highest level of conductivity among the tested electrolytes, TNM analysis was meticulously carried out. The aim was to discern whether this electrolyte holds promise for integration into energy devices. The TNM analysis took place under standard room temperature conditions, offering a comprehensive examination of how specific charge carriers, whether ions or electrons contribute to the overall behavior of the electrolyte.

The ensuing Fig. 15 encapsulates a wealth of information. Initially, there is a marked and abrupt drop in the initial current (I_i), followed by the attainment of a steady-state current (I_{ss}) commencing at the 80th second and persisting thereafter. This initial current drop is attributed to the limited mobility of ions, where the character of the stainless-steel electrode impedes ion diffusion. During this phase, only electrons are permitted to partake in the transport mechanism. The notable surge in current at the outset is due to the joint involvement of ions and electrons. Initially, cations and anions migrate in opposite directions toward the electrode surface from the electrolyte's bulk, forming a double-layer at the electrode-electrolyte interfaces. This process leads to polarization. The polarization of the cell ends when it reaches a stable state, with the subsequent current flow being solely attributable to electrons. This shift to electron-dominant transport is the basis for determining the electron transference number ($t_{electron}$) using stainless-steel electrodes. As time progresses, the establishment of diffusion layers on the electrode interface becomes instrumental in generating a steady state of current. These diffusion layers give rise to a substantial resistance within a passive ionic layer. Consequently, ions are no longer significant contributors to the current flow within this region. Once ions have been effectively reduced, a consistent current flow ensues, driven exclusively by electrons.

It is well established that the cation conductivity in the polymer-based electrolyte is significantly higher compared to anions, resulting in a much higher transference number for cations. This observation implies that the achieved ion transference number in this study is predominantly influenced by

Fig. 15 The current versus time plot for the CPLCG5 electrolyte
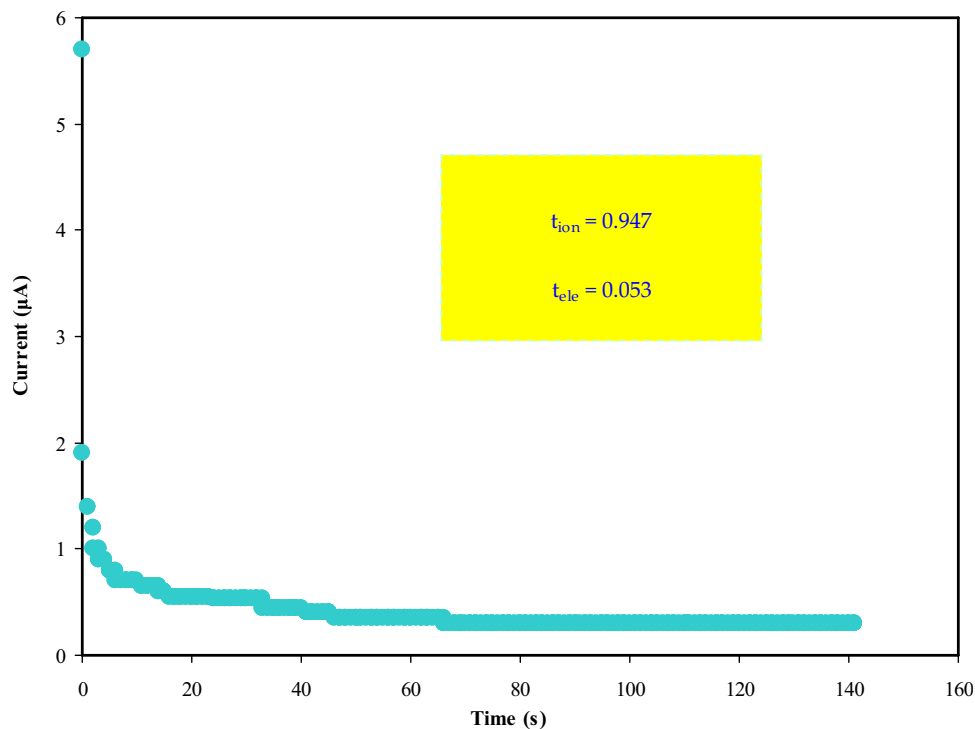
the mobility of lithium (Li$^+$) ions in the electrolyte. Concerning the role of anions, it is reasonable that they form strong electrostatic interactions or are covalently linked to the hydroxyl FGs in the host matrix medium. This may lead to the anions being less involved in ion transport or ion-electron polarization, especially if they are large-sized bulk anions. Transference numbers, quantified as the ion transference number (t_{ion}) and the electron transference number ($t_{electron}$), were calculated for the CPLCG5 electrolyte employing specific equations. Remarkably, the CPLCG5 electrolyte achieved a notably high t_{ion} value of 0.947, strongly indicating the predominant role of ions within the system [77]. A similar observation has been corroborated by previous studies, notably by Shukur et al. [38], which suggests that a t_{ion} value approaching unity signifies ions as the principal carriers of charge in the system. This consistent observation has been reported by other researchers, such as Rama et al. [78] and Tang et al. [79]. In summary, TNM analysis offers an insightful glimpse into the dynamic behavior of charge carriers within CPLCG5, providing a foundation for assessing its suitability for integration into energy devices.

LSV Study

Determining the breakdown potential of CPLCG5 through LSV is of great significance when evaluating its suitability for incorporation into energy storage systems such as solar cells, batteries, and supercapacitors [48]. Knowing the potential at which the electrolyte may experience oxidation and initiate degradation is essential for ensuring the durability and continued efficiency of these devices. As depicted in Fig. 16, the electrolyte exhibits remarkable stability, with no discernible changes in current observed below a potential of 3.10 V. However, beyond this threshold, a sharp increase in current becomes evident. This increase is attributed to the disruption of interactions between polymer chains and between the polymer and salt components, ultimately leading to polymer degradation [52].

The findings presented in this study indicate that the present system exhibits a reasonably broad electrochemical potential window before experiencing degradation. This window is wider compared to many other aqueous electrolytes but does not reach the broader potential range typically associated with ionic liquid (IL) electrolytes, which typically span from 3.5 to 4 V [80]. For instance, in previous studies, ((PEO–PMMA)– LiClO$_4$–3 wt% nanofiller) was reported to remain stable up to 3.05 V [81]. Similarly, S Rudhziah. reported that CMKC/CMCE SPE demonstrated stability below 2.0 V [82]. The findings from this research align with those of previous studies focusing on magnesium-based electrolytes and suggest that the CPLCG5 electrolyte possesses the requisite stability for incorporation into Energy Density Layer Capacitors (EDLCs). This promising result positions CPLCG5 as a viable candidate for various ESAs, given its favorable electrochemical potential window and potential for long-term reliability in demanding operational environments.

Fig. 16 The measured LSV plot for the CPLCG5 system
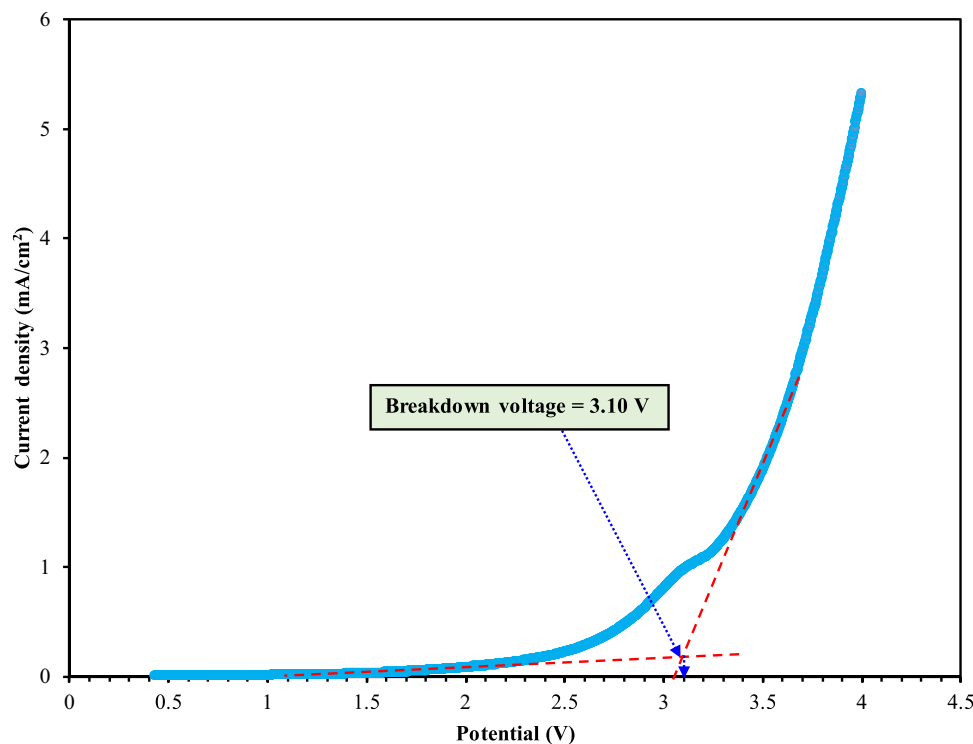
Cyclic Voltammetry

The cyclic voltammetry analysis of the assembled EDLC consisting of with activated carbon and CPLCG5 reveals scan-rate-dependent behavior. The absence of distinct peaks in the CV plot confirms the predominantly capacitive nature of the device. The observed capacitance values are in line with the expected trends, reflecting the varying response of the EDLC at different scan rates, and are indicative of its performance characteristics in terms of ion accumulation and resistance. It is a well-established fact that the behavior of a capacitor, in this case, an EDLC, is influenced by the scan rate used during CV experiments. Therefore, multiple scan rates, specifically 20, 50, and 100 mV/s, were employed to thoroughly examine its characteristics. In Fig. 17, the shape of the CV plot undergoes distinctive changes, ranging from rectangular to leaf-like shapes, without any conspicuous peaks. According to the findings of Jäckel et al. [83], the presence of peaks in a CV plot typically indicates the occurrence of Faradaic current, which is associated with processes like intercalation and deintercalation. Such processes are not expected to take place in a capacitor like an EDLC. At increased scan rates, the motion of mobile ions within the system takes place quickly. Moreover, because of factors like internal resistance and the porous characteristics of the carbon electrode material, the correlation between voltage and current becomes contingent on the pace of ion movement [40].

The capacitance values of the EDLC, as outlined in Table 6, provide valuable insights. Notably, the capacitance

Table 6 Changes in capacitance values in relation to various scan rates

Scan rate (mV/s)	Capacitance (F/g)
100	12.92
50	22.59
20	38.68

(C_{spc}) is more substantial at lower scan rates and decreases as the scan rate increases. This behavior is consistent with expectations: at lower scan rates, the CV response tends to exhibit relatively flat plateaus, indicating the accumulation of ions at the electrode-electrolyte interface and low ohmic resistance, as exemplified in Fig. 17 [84, 85]. Table 7 displays the findings of various polymer-based electrolytes containing different dopant salts utilized in EDLC devices. These results are contrasted with the outcomes of our study, focusing on potential stability, ion transference number, and specific capacitance. Fortunately, the electrolyte prepared in this study exhibits favorable performance, making it suitable for applications in energy storage devices like EDLC. Notably, its performance surpasses many other studies documented in the literature.

Conclusion

To sum up, concentrated on biopolymer blend electrolytes plasticized with glycerol, emphasizing Li^+ ion conductivity and employing various techniques. FTIR analysis

Fig. 17 Alterations in the shapes of cyclic voltammetry (CV) plots as the scan rate is modified in the constructed EDLC.
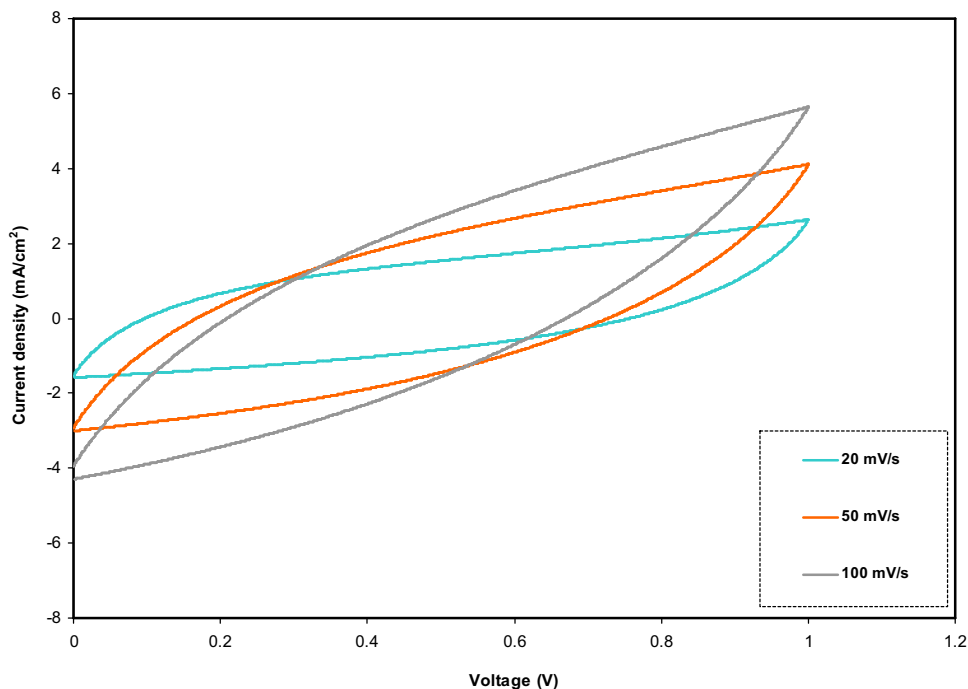
Table 7 Comparing the results of some previous works with the present work

Systems	C_{spc}(F/g)	ESW (V)	t_{ion}	Ref
Dextran:NH$_4$Br	2.46	1.62	0.92	[86]
Corn Starch:LiClO$_4$:SiO$_2$	8.71	2.5	–	[87]
MX:MC:NH$_4$Br: [Emim]Br	9.47	1.56	0.99	[88]
CS:MC:NH$_4$I	9.97	2.2	0.97	[89]
PVA:LiClO$_4$:TiO$_2$	12.5	2.3	–	[90]
PVA:CH$_3$COONH$_4$:BmImBr	21.89	2.0	–	[91]
PVA:CS:NH$_4$NO$_3$:EC	27.1	1.7	–	[92]
PDMA: MgTf$_2$: Co$_3$O$_4$	29.48	–	0.98	[93]
CS:PVA:NaBr:GL:Al$_2$O$_3$	**38.68**	**3.1**	**0.947**	**Present work**

underscored the substantial impact of glycerol on polymer-salt interactions, with a shift in FTIR bands indicating an increase in free ions within the electrolyte films. EIS measurements revealed that the addition of glycerol reduced bulk resistance and enhanced conductivity simultaneously. The EEC model provided a comprehensive view of the entire electrolyte system, equating it to realistic circuit elements for better visualization. Calculated DC conductivity values confirmed the suitability of these films for ESAs with a maximum conductivity of 2.01×10^{-4} S cm^{-1}. Furthermore, the high ϵ' and ϵ'' values at low frequencies suggested interfacial polarization and charge accumulation. The shifting of tanδ peaks to higher frequencies and their broadening indicated enhanced cation mobility with non-Debye behavior. The combination of the tan δ graph with the Argand plot revealed that ion conduction happens through both viscoelastic and conductivity relaxation, depending on the concentration of glycerol in the prepared electrolyte system. Electrochemical studies indicated the suitability of the film for EDLC application, supported by a favorable TNM value for ions and a decomposition voltage of 3.1 V. CV curves at different scan rates demonstrated a well-designed EDLC device, exhibiting no signs of redox peaks and high capacitance values ranging from 12.92 F/g to 38.68 F/g. Overall, our findings suggest that these biopolymer blend electrolytes have great promise as effective materials for energy storage and EDLC applications.

Author Contributions Conceptualization, SB; Data curation, RT; Formal analysis, DM, SB and RT; Funding acquisition, BA; Investigation, RT, SA and PS; Methodology, SA, HJ, RT and AA; Project administration, SB and MF; Resources, BA and HJ ; Supervision, SB and MK; Validation, DM, SA, PS, WO, BA, AA and HJ ; Visualization, DM and RT; Writing—original draft, DM and SB; Writing—review & editing, RT, SA, WO, PS, HJ, and A

Declarations

Conflict of interest The authors assert that they have no conflicts of interest to disclose.

References

1. Ma X, Yu J, He K, Wang N (2007) The effects of different plasticizers on the properties of thermoplastic starch as solid polymer electrolytes. Macromol Mater Eng 292:503–510. https://doi.org/10.1002/mame.200600445

2. Ma X, Yu J, Zhao A (2006) Properties of biodegradable poly(propylene carbonate)/starch composites with succinic anhydride. Compos Sci Technol 66:2360–2366. https://doi.org/10.1016/j.compscitech.2005.11.028

3. Yoon S, Ahmed F, Zhang W, Ryu T, Jin L, Kim D et al (2020) Flexible blend polymer electrolyte membranes with excellent conductivity for fuel cells. Int J Hydrogen Energy 45:27611–27621. https://doi.org/10.1016/j.ijhydene.2020.07.076

4. Li L, Wang F, Li J, Yang X, You J (2017) Electrochemical performance of gel polymer electrolyte with ionic liquid and PUA/PMMA prepared by ultraviolet curing technology for lithium-ion battery. Int J Hydrogen Energy 42:12087–12093. https://doi.org/10.1016/j.ijhydene.2017.02.085

5. Zainuddin NK, Rasali NMJ, Mazuki NF, Saadiah MA, Samsudin AS (2020) Investigation on favourable ionic conduction based on CMC-K carrageenan proton conducting hybrid solid bio-polymer electrolytes for applications in EDLC. Int J Hydrogen Energy 45:8727–8741. https://doi.org/10.1016/j.ijhydene.2020.01.038

6. Singh R, Singh PK, Singh V, Bhattacharya B (2019) Quantitative analysis of ion transport mechanism in biopolymer electrolyte. Opt Laser Technol 113:303–309. https://doi.org/10.1016/j.optlastec.2018.12.036

7. Saadiah MA, Nagao Y, Samsudin AS (2021) Enhancement on protonation (H+) with incorporation of flexible ethylene carbonate in CMC–PVA–30 wt % NH4NO3 film. Int J Hydrogen Energy 46:17231–17245. https://doi.org/10.1016/j.ijhydene.2021.02.187

8. Zhou K, Zhang M, Zhang X, Wang T, Wang H, Wang Z et al (2023) A cellulose reinforced polymer composite electrolyte for the wide-temperature-range solid lithium batteries. Chem Eng J 464:142537. https://doi.org/10.1016/j.cej.2023.142537

9. Isa MIN, Sohaimy MIH, Ahmad NH (2021) Carboxymethyl cellulose plasticized polymer application as bio-material in solid-state

hydrogen ionic cell. Int J Hydrogen Energy 46:8030–8039. https://doi.org/10.1016/j.ijhydene.2020.11.274

10. Nadirah BN, Ong CC, Saheed MSM, Yusof YM, Shukur MF (2020) Structural and conductivity studies of polyacrylonitrile/methylcellulose blend based electrolytes embedded with lithium iodide. Int J Hydrogen Energy 45:19590–19600. https://doi.org/10.1016/j.ijhydene.2020.05.016

11. Ben youcef H, Henkensmeier D, Balog S, Scherer GG, Gubler L (2020) Copolymer synergistic coupling for chemical stability and improved gas barrier properties of a polymer electrolyte membrane for fuel cell applications. Int J Hydrogen Energy 45:7059–7068. https://doi.org/10.1016/j.ijhydene.2019.12.208

12. Majumdar S, Sen P, Ray R (2019) Ionic interactions and transport properties in chitosan-starch based blend solid biopolymer electrolytes. Mater Today Proc 18:4913–4920. https://doi.org/10.1016/j.matpr.2019.07.483

13. Liang YF, Xia Y, Zhang SZ, Wang XL, Xia XH, Gu CD et al (2019) A preeminent gel blending polymer electrolyte of poly(vinylidene fluoride-hexafluoropropylene) -poly(propylene carbonate) for solid-state lithium ion batteries. Electrochim Acta 296:1064–1069. https://doi.org/10.1016/j.electacta.2018.11.182

14. Thayumanasundaram S, Rangasamy VS, Seo JW, Locquet JP (2017) Electrochemical performance of polymer electrolytes based on poly(vinyl alcohol)/Poly(acrylic acid) blend and pyrrolidinium ionic liquid for lithium rechargeable batteries. Electrochim Acta 240:371–378. https://doi.org/10.1016/j.electacta.2017.04.107

15. Abdulwahid RT, Aziz SB, Kadir MFZ (2023) Replacing synthetic polymer electrolytes in energy storage with flexible biodegradable alternatives : sustainable green biopolymer blend electrolyte for supercapacitor device. Mater Today Sustain 23:100472. https://doi.org/10.1016/j.mtsust.2023.100472

16. Abdulwahid RT, Aziz SB, Kadir MFZ (2023) Environmentally friendly plasticized electrolyte based on chitosan (CS): Potato starch (PS) polymers for EDLC application: steps toward the greener energy storage devices derived from biopolymers. J Energy Storage 67:107636. https://doi.org/10.1016/j.est.2023.107636

17. Aziz SB, Abidin ZHZ, Arof AK (2010) Influence of silver ion reduction on electrical modulus parameters of solid polymer electrolyte based on chitosansilver triflate electrolyte membrane. Express Polym Lett 4:300–310. https://doi.org/10.3144/expresspolymlett.2010.38

18. Aziz SB, Abdullah OG, Rasheed MA, Ahmed HM (2017) Effect of high salt concentration (HSC) on structural, morphological, and electrical characteristics of chitosan based solid polymer electrolytes. Polym (Basel) 9:187. https://doi.org/10.3390/polym9060187

19. Yassin AY (2021) Impedance, structural and thermal analyses of polyvinyl alcohol/polyvinyl pyrrolidone blend incorporated with Li + ions for lithium-ion batteries. J Mater Res Technol 15:754–767. https://doi.org/10.1016/j.jmrt.2021.08.063

20. Salem AM, Mohamed AR, Yassin AY (2023) The effect of low concentrations of polypyrrole on the structural, thermal, and dielectric characteristics of CMC/PPy blends. J Mater Sci Mater Electron 34:1–13. https://doi.org/10.1007/s10854-023-10938-1

21. Yassin AY (2023) Synthesized polymeric nanocomposites with enhanced optical and electrical properties based on gold nanoparticles for optoelectronic applications. J Mater Sci Mater Electron 34:1–18. https://doi.org/10.1007/s10854-022-09402-3

22. Damoom MM, Saeed A, Alshammari EM, Alhawsawi AM, Yassin AY, Abdulwahed JAM et al (2023) The role of TiO2 nanoparticles in enhancing the structural, optical, and electrical properties of PVA/PVP/CMC ternary polymer blend: nanocomposites for capacitive energy storage. J Sol-Gel Sci Technol 108:742–755. https://doi.org/10.1007/s10971-023-06223-6

23. Al-Muntaser AA, Pashameah RA, Saeed A, Alwafi R, Alzahrani E, AlSubhi SA et al (2023) Boosting the optical, structural, electrical, and dielectric properties of polystyrene using a hybrid GNP/Cu nanofiller: novel nanocomposites for energy storage applications. J Mater Sci Mater Electron. https://doi.org/10.1007/s10854-023-10104-7

24. Gupta S, Varshney PK (2017) Effect of plasticizer concentration on structural and electrical properties of hydroxyethyl cellulose (HEC)-based polymer electrolyte. Ionics (Kiel) 23:1613–1617. https://doi.org/10.1007/s11581-017-2116-8

25. Kumar R, Sharma S, Pathak D, Dhiman N, Arora N (2017) Ionic conductivity, FTIR and thermal studies of nano-composite plasticized proton conducting polymer electrolytes. Solid State Ionics 305:57–62. https://doi.org/10.1016/j.ssi.2017.04.020

26. Shin JH, Jung SS, Kim KW, Ahn HJ, Ahn JH (2002) Preparation and characterization of plasticized polymer electrolytes based on the PVdF-HFP copolymer for lithium/sulfur battery. J Mater Sci Mater Electron 13:727–733. https://doi.org/10.1023/A:1021521207247

27. Richardson PM, Voice AM, Ward IM (2014) Two distinct lithium diffusive species for polymer gel electrolytes containing LiBF4, propylene carbonate (PC) and PVDF. Int J Hydrogen Energy 39:2904–2908. https://doi.org/10.1016/j.ijhydene.2013.04.102

28. Woo HJ, Majid SR, Arof AK (2013) Effect of ethylene carbonate on proton conducting polymer electrolyte based on poly(ε-caprolactone) (PCL). Solid State Ionics 252:102–108. https://doi.org/10.1016/j.ssi.2013.07.005

29. Chai MN, Isa MIN (2016) Novel Proton Conducting Solid Biopolymer Electrolytes based on Carboxymethyl Cellulose Doped with oleic acid and plasticized with glycerol. Sci Rep 6:27328. https://doi.org/10.1038/srep27328

30. Yusof YM, Kadir MFZ (2016) Electrochemical characterizations and the effect of glycerol in biopolymer electrolytes based on methylcellulose-potato starch blend. Mol Cryst Liq Cryst 627:220–233. https://doi.org/10.1080/15421406.2015.1137115

31. Shukur MF, Ithnin R, Illias HA, Kadir MFZ (2013) Proton conducting polymer electrolyte based on plasticized chitosan-PEO blend and application in electrochemical devices. Opt Mater (Amst) 35:1834–1841. https://doi.org/10.1016/j.optmat.2013.03.004

32. Dragunski DC, Pawlicka A (2002) Starch based solid polymeric electrolytes. Mol Cryst Liq Cryst Sci Technol Sect A Mol Cryst Liq Cryst 374:561–568. https://doi.org/10.1080/10587250210443

33. Bandara TMWJ, Dissanayake MAKL, Albinsson I, Mellander BE (2011) Mobile charge carrier concentration and mobility of a polymer electrolyte containing PEO and Pr4N + I- using electrical and dielectric measurements. Solid State Ionics 189:63–68. https://doi.org/10.1016/j.ssi.2011.03.004

34. Rice MJ, Roth WL (1972) Ionic transport in super ionic conductors: a theoretical model. J Solid State Chem 4:294–310. https://doi.org/10.1016/0022-4596(72)90121-1

35. Aziz SB, Karim WO, Brza MA, Abdulwahid RT, Saeed SR, Al-Zangana S et al (2019) Ion transport study in CS: POZ based polymer membrane electrolytes using Trukhan model. Int J Mol Sci. https://doi.org/10.3390/ijms20215265

36. Arof AK, Amirudin S, Yusof SZ, Noor IM (2014) A method based on impedance spectroscopy to determine transport properties of polymer electrolytes. Phys Chem Chem Phys 16:1856–1867. https://doi.org/10.1039/c3cp53830c

37. Abdulwahid RT, Aziz SB, Kadir MFZ (2022) Design of proton conducting solid biopolymer blend electrolytes based on chitosan-potato starch biopolymers : deep approaches to structural and ion relaxation dynamics of H + ion. J Appl Polym Sci 139:e52892. https://doi.org/10.1002/app.52892

38. Shukur MF, Ithnin R, Kadir MFZ (2016) Ionic conductivity and dielectric properties of potato starch-magnesium acetate

biopolymer electrolytes: the effect of glycerol and 1-butyl-3-meth-ylimidazolium chloride. Ionics (Kiel) 22:1113–1123. https://doi.org/10.1007/s11581-015-1627-4

39. Ibrahim S, Mohd Yasin SM, Nee NM, Ahmad R, Johan MR (2012) Conductivity and dielectric behaviour of PEO-based solid nanocomposite polymer electrolytes. Solid State Commun 152:426–434. https://doi.org/10.1016/j.ssc.2011.11.037

40. Liew CW, Ramesh S, Arof AK (2016) Enhanced capacitance of EDLCs (electrical double layer capacitors) based on ionic liquid-added polymer electrolytes. Energy 109:546–556. https://doi.org/10.1016/j.energy.2016.05.019

41. Mohit, Hashmi SA (2023) Biodegradable poly-ε-caprolactone based porous polymer electrolytes for high performance super-capacitors with carbon electrodes. J Power Sources 557:232548. https://doi.org/10.1016/j.jpowsour.2022.232548

42. Pistorius AMA, DeGrip WJ (2004) Deconvolution as a tool to remove fringes from an FT-IR spectrum. Vib Spectrosc 36:89–95. https://doi.org/10.1016/j.vibspec.2004.04.001

43. Xi J, Bai Y, Qiu X, Zhu W, Chen L, Tang X (2005) Conductivities and transport properties of microporous molecular sieves doped composite polymer electrolyte used for lithium polymer battery. New J Chem 29:1454–1460. https://doi.org/10.1039/b505332c

44. Abarna S, Hirankumar G (2017) Electrical, dielectric and electro-chemical studies on new Li ion conducting solid polymer electro-lytes based on polyethylene glycol p-tert-octylphenyl ether. Polym Sci - Ser A 59:660–668. https://doi.org/10.1134/S0965545X17050017

45. Ramlli MA, Bashirah NAA, Isa MIN (2018) Ionic conductivity and structural analysis of 2-hyroxyethyl cellulose doped with gly-colic acid solid Biopolymer Electrolytes for Solid Proton Battery. IOP Conf Ser Mater Sci Eng 440:012038. https://doi.org/10.1088/1757-899X/440/1/012038

46. Brza MA, Aziz SB, Anuar H, Ali F (2020) Structural, ion trans-port parameter and electrochemical properties of plasticized poly-mer composite electrolyte based on PVA: a novel approach to fab-ricate high performance EDLC devices. Polym Test 91:106813. https://doi.org/10.1016/j.polymertesting.2020.106813

47. Aniskari NAB, Mohd Isa MIN, Bin (2017) The effect of ionic charge carriers in 2-hydroxyethyl cellulose solid biopolymer elec-trolytes doped glycolic acid via FTIR-deconvolution technique. J Sustain Sci Manag 2017:71–79

48. Mahato DK, Dutta A, Sinha TP (2010) Impedance spectroscopy analysis of double perovskite Ho 2NiTiO6. J Mater Sci 45:6757–6762. https://doi.org/10.1007/s10853-010-4771-2

49. Rawat P, Saroj AL (2023) Effect of ionic liquid on plasticized CS-PVP-NaI based bio-polymer blend electrolytes: structural, thermal, dielectric and ion transport properties study. Mater Sci Eng B Solid-State Mater Adv Technol 288:116215. https://doi.org/10.1016/j.mseb.2022.116215

50. Hamsan MH, Shukur MF, Kadir MFZ (2017) NH4NO3 as charge carrier contributor in glycerolized potato starch-methyl cellulose blend-based polymer electrolyte and the application in electro-chemical double-layer capacitor. Ionics (Kiel) 23:3429–3453. https://doi.org/10.1007/s11581-017-2155-1

51. Abdullah AM, Aziz SB, Brza MA, Saeed SR, Al-Asbahi BA, Sadiq NM et al (2022) Glycerol as an efficient plasticizer to increase the DC conductivity and improve the ion transport parameters in biopolymer based electrolytes: XRD, FTIR and EIS studies. Arab J Chem 15:103791. https://doi.org/10.1016/j.arabjc.2022.103791

52. Aziz SB, Woo TJ, Kadir MFZ, Ahmed HM (2018) A conceptual review on polymer electrolytes and ion transport models. J Sci Adv Mater Devices 3:1–17. https://doi.org/10.1016/j.jsamd.2018.01.002

53. Aziz SB, Abdulwahid RT, Kadir MFZ, Ghareeb HO, Ahamad T, Alshehri SM (2021) Design of non-faradaic EDLC from

plasticized MC based Polymer electrolyte with an energy density close to lead-acid batteries. J Ind Eng Chem 105:414–426. https://doi.org/10.1016/j.jiec.2021.09.042

54. Abdullah AM, Aziz SB, Saeed SR (2021) Structural and electri-cal properties of polyvinyl alcohol (PVA):Methyl cellulose (MC) based solid polymer blend electrolytes inserted with sodium iodide (NaI) salt. Arab J Chem 14:103388. https://doi.org/10.1016/j.arabjc.2021.103388

55. Teoh KH, Lim CS, Ramesh S (2014) Lithium ion conduction in corn starch based solid polymer electrolytes. Measurement 48:87–95. https://doi.org/10.1016/j.measurement.2013.10.040

56. Liew C, Ramesh S (2015) Electrical, structural, thermal and elec-trochemical properties of corn starch-based biopolymer electro-lytes. Carbohydr Polym 124:222–228. https://doi.org/10.1016/j.carbpol.2015.02.024

57. Teoh KH, Lim CS, Liew CW, Ramesh S (2016) Preparation and performance analysis of barium titanate incorporated in corn starch-based polymer electrolytes for electric double layer capac-itor application. J Appl Polym Sci 133:1–8. https://doi.org/10.1002/app.43275

58. Pal P, Ghosh A (2016) Dynamics and relaxation of charge car-riers in poly(methylmethacrylate)-lithium salt based Polymer electrolytes plasticized with ethylene carbonate. J Appl Phys 120:045108. https://doi.org/10.1063/1.4959985

59. Shukla N, Thakur AK, Shukla A, Marx DT (2014) Ion conduc-tion mechanism in solid polymer electrolyte: an applicability of almond-west formalism. Int J Electrochem Sci 9:7644–7659

60. Choudhary S, Sengwa RJ (2015) Structural and dielectric studies of amorphous and semicrystalline polymers blend-based nano-composite electrolytes. J Appl Polym Sci 132:23–29. https://doi.org/10.1002/app.41311

61. Arya A, Sharma S, Sharma AL, Kumar D, Sadiq M (2016) Struc-tural and dielectric Behaviour of Blend Polymer Electrolyte based on PEO-PAN + LiPF6. Asian J Eng Appl Technol 5:4–7. https://doi.org/10.51983/ajeat-2016.5.1.774

62. Bhargav PB, Mohan VM, Sharma AK, Rao VVRN (2009) Inves-tigations on electrical properties of (PVA:NaF) Polymer elec-trolytes for electrochemical cell applications. Curr Appl Phys 9:165–171. https://doi.org/10.1016/j.cap.2008.01.006

63. Ahad N, Saion E, Gharibshahi E, Structural T (2012) Electrical properties of PVA-Sodium Salicylate Solid Composite Polymer Electrolyte. J Nanomater 2012:857569. https://doi.org/10.1155/2012/857569

64. Yu X, Yi B, Liu F, Wang X (2008) Prediction of the dielectric dissipation factor tan δ of polymers with an ANN model based on the DFT calculation. React Funct Polym 68:1557–1562. https://doi.org/10.1016/j.reactfunctpolym.2008.08.009

65. Jiang H, Hong L, Venkatasubramanian N, Grant JT, Eyink K, Wiacek K et al (2007) The relationship between chemical struc-ture and dielectric properties of plasma-enhanced chemical vapor deposited polymer thin films. Thin Solid Films 515:3513–3520. https://doi.org/10.1016/j.tsf.2006.10.126

66. Baskaran R, Selvasekarapandian S, Hirankumar G, Bhuvaneswari MS (2004) Dielectric and conductivity relaxations in PVAc based Polymer electrolytes. Ionics (Kiel) 10:129–134. https://doi.org/10.1007/BF02410321

67. Idris NH, Senin HB, Arof AK (2007) Dielectric spectra of LiTFSI-doped chitosan/PEO blends. Ionics (Kiel) 13:213–217. https://doi.org/10.1007/s11581-007-0093-z

68. Smaoui H, Mir LEL, Guermazi H, Agnel S, Toureille A (2009) Study of dielectric relaxations in zinc oxide-epoxy resin nanocom-posites. J Alloys Compd 477:316–321. https://doi.org/10.1016/j.jallcom.2008.10.084

69. Aziz SB (2016) Occurrence of electrical percolation threshold and observation of phase transition in chitosan (1 − x) :AgI x (0.05 ≤ x ≤ 0.2)-based ion-conducting solid polymer composites.

Appl Phys a Mater Sci Process 122:706. https://doi.org/10.1007/s00339-016-0235-0

70. Aziz SB, Abidin ZHZ (2015) Ion-transport study in nanocomposite solid polymer electrolytes based on chitosan: Electrical and dielectric analysis. J Appl Polym Sci 132:1–10. https://doi.org/10.1002/app.41774

71. Belattar J, Graça MPF, Costa LC, Achour ME, Brosseau C (2010) Electric modulus-based analysis of the dielectric relaxation in carbon black loaded polymer composites. J Appl Phys. https://doi.org/10.1063/1.3452366

72. Pradhan DK, Choudhary RNP, Samantaray BK (2008) Studies of dielectric relaxation and AC conductivity behavior of plasticized polymer nanocomposite electrolytes. Int J Electrochem Sci 3:597–608

73. Sengwa RJ, Choudhary S, Sankhla S (2008) Low frequency dielectric relaxation processes and ionic conductivity of montmorillonite clay nanoparticles colloidal suspension in poly(vinyl pyrrolidone)-ethylene glycol blends. Express Polym Lett 2:800–809. https://doi.org/10.3144/expresspolymlett.2008.93

74. Aziz SB, Abdullah OG, Rasheed MA (2017) Structural and electrical characteristics of PVA:NaTf based solid polymer electrolytes: role of lattice energy of salts on electrical DC conductivity. J Mater Sci Mater Electron 28:12873–12884. https://doi.org/10.1007/s10854-017-7117-x

75. Marzantowicz M, Dygas JR, Krok F, Florja??czyk Z, Zygad??o-Monikowska E (2007) Conductivity and dielectric properties of polymer electrolytes PEO:LiN(CF3SO2)2 near glass transition. J Non Cryst Solids 353:4467–4473. https://doi.org/10.1016/j.jnoncrysol.2007.04.046

76. Mohomed K, Gerasimov TG, Moussy F, Harmon JP (2005) A broad spectrum analysis of the dielectric properties of poly(2-hydroxyethyl methacrylate). Polym (Guildf) 46:3847–3855. https://doi.org/10.1016/j.polymer.2005.02.100

77. Basha SS, Rao MR (2019) Spectroscopic and Electrochemical properties of (1-x)[PVA/PVP]:x [MgCl2{6H2O}] Blend Polymer Electrolyte films. Int J Polym Sci 75:2926167

78. Rama Mohan K, Achari VBS, Rao VVRN, Sharma AK (2011) Electrical and optical properties of (PEMA/PVC) polymer blend electrolyte doped with NaClO4. Polym Test 30:881–886. https://doi.org/10.1016/j.polymertesting.2011.08.010

79. Tang J, Muchakayala R, Song S, Wang M, Kumar KN (2016) Effect of EMIMBF4 ionic liquid addition on the structure and ionic conductivity of LiBF4-complexed PVdF-HFP polymer electrolyte films. Polym Test 50:247–254. https://doi.org/10.1016/j.polymertesting.2016.01.023

80. Polu AR, Rhee HW, Kim DK (2015) New solid polymer electrolytes (PEO20–LiTDI–SN) for lithium batteries: structural, thermal and ionic conductivity studies. J Mater Sci Mater Electron 26:8548–8554. https://doi.org/10.1007/s10854-015-3527-9

81. Dhatarwal P, Choudhary S, Sengwa RJ (2018) Electrochemical performance of Li+-ion conducting solid polymer electrolytes based on PEO–PMMA blend matrix incorporated with various inorganic nanoparticles for the lithium ion batteries. Compos Commun 10:11–17. https://doi.org/10.1016/j.coco.2018.05.004

82. Rudhziah S, Rani MSA, Ahmad A, Mohamed NS, Kaddami H (2015) Potential of blend of kappa-carrageenan and cellulose derivatives for green polymer electrolyte application. Ind Crops Prod 72:133–141. https://doi.org/10.1016/j.indcrop.2014.12.051

83. Jäckel N, Rodner M, Schreiber A, Jeongwook J, Zeiger M, Aslan M et al (2016) Anomalous or regular capacitance? The influence of pore size dispersity on double-layer formation. J Power Sources 326:660–671. https://doi.org/10.1016/j.jpowsour.2016.03.015

84. He X, Lei J, Geng Y, Zhang X, Wu M, Zheng M (2009) Preparation of microporous activated carbon and its electrochemical performance for electric double layer capacitor. J Phys Chem Solids 70:738–744. https://doi.org/10.1016/j.jpcs.2009.03.001

85. Fang B, Binder L (2006) A novel carbon electrode material for highly improved EDLC performance. J Phys Chem B 110:7877–7882. https://doi.org/10.1021/jp060110d

86. Hamsan MH, Shukur MF, Aziz SB, Yusof YM, Kadir MFZ (2020) Influence of NH4Br as an ionic source on the structural/electrical properties of dextran-based biopolymer electrolytes and EDLC application. Bull Mater Sci. https://doi.org/10.1007/s12034-019-2008-9

87. Teoh KH, Lim CS, Liew CW, Ramesh S, Ramesh S (2015) Electric double-layer capacitors with corn starch-based biopolymer electrolytes incorporating silica as filler. Ionics (Kiel) 21:2061–2068. https://doi.org/10.1007/s11581-014-1359-x

88. Asnawi ASFM, Hamsan MH, Kadir FZ, Aziz SB, Matmin J (2021) Impregnation of [Emim]Br ionic liquid as plasticizer in biopolymer electrolytes for EDLC application. Electrochim Acta 375:137923. https://doi.org/10.1016/j.electacta.2021.137923

89. Aziz SB, Hamsan MH, Brza MA, Kadir MFZ, Muzakir SK, Abdulwahid RT (2020) Effect of glycerol on EDLC characteristics of chitosan:methylcellulose polymer blend electrolytes. J Mater Res Technol 9:8355–8366. https://doi.org/10.1016/j.jmrt.2020.05.114

90. Lim CS, Teoh KH, Liew CW, Ramesh S (2014) Capacitive behavior studies on electrical double layer capacitor using poly (vinyl alcohol)-lithium perchlorate based Polymer electrolyte incorporated with TiO2. Mater Chem Phys 143:661–667. https://doi.org/10.1016/j.matchemphys.2013.09.051

91. Liew CW, Ramesh S, Arof AK (2015) Characterization of ionic liquid added poly(vinyl alcohol)-based proton conducting polymer electrolytes and electrochemical studies on the supercapacitors. Int J Hydrogen Energy 40:852–862. https://doi.org/10.1016/j.ijhydene.2014.09.160

92. Kadir MFZ, Arof AK (2013) Application of PVA-chitosan blend polymer electrolyte membrane in electrical double layer capacitor. Mater Res Innov 15:S217–S220. https://doi.org/10.1179/143307511X13031890749299

93. Bashir S, Omar FS, Hina M, Numan A, Iqbal J, Ramesh S et al (2020) Synthesis and characterization of hybrid poly (N, N-dimethylacrylamide) composite hydrogel electrolytes and their performance in supercapacitor. Electrochim Acta 332:135438. https://doi.org/10.1016/j.electacta.2019.135438